Modern Trends in Tungsten Alloys Electrodeposition with Iron Group Metals

N. Tsyntsaru[a,b], H. Cesiulis[c], M. Donten[d], J. Sort[e], E. Pellicer[f], E. J. Podlaha-Murphy[g]

[a] *Katholieke Universiteit Leuven, Department MTM, Belgium*
[b] *Institute of Applied Physics, Academy of Sciences of Moldova, Chisinau, MD-2028, Moldova*
[c] *Vilnius University, Dept. Phys. Chem., Naugarduko 24, Vilnius LT-03225, Lithuania, e-mail: henrikas.cesiulis@chf.vu.lt*
[d] *Faculty of Chemistry, University of Warsaw Pasteura 1, 02-093, Warsaw, Poland*
[e] *Institució Catalana de Recerca i Estudis Avançats (ICREA) and Departament de Física, Universitat Autònoma de Barcelona, E-08193, Bellaterra, Spain*
[f] *Departament de Física, Universitat Autònoma de Barcelona, E-08193, Bellaterra, Spain*
[g] *Department of Chemical Engineering, Northeastern University, Boston, MA 02115, USA*

Theoretical and applied studies of tungsten alloys with iron group metals (Me-W) are being carried out worldwide, in the light of their versatile applications. The aim of this paper is to provide an overview of the works on electrodeposition of tungsten alloys with iron group metals, their properties and applications. There are 221 papers reviewing on the following theoretical and practical topics: chemistry of electrolytes used for electrodeposition, codeposition mechanisms, and properties of electrodeposited tungsten alloys. In addition, the formation of W(VI) and iron group metal (Me) complexes (polytungstates and complexes of Me(II) and W(VI)) with citrates and OH^- is analysed based on the published data and the calculated distribution of species as a function of pH (ranged from 1 to 10) is provided for solutions with/without citrates. The adduced data are correlated with the compositions of electrodeposited alloys. Various codeposition models of tungsten with iron group metals described in the literature are critically discussed as well. The peculiarities of the structure of tungsten alloys and their thermal stability, mechanical, tribological, and magnetic properties, corrosion of alloys, their applications in hydrogen electrocatalysis, template-assisted deposition into recesses (aimed to obtain micro- and nanostructures) are also reviewed and mapped.

УДК 541.138:2+620.3

INTRODUCTION

The interest in tungsten and its alloys has been driven by its outstanding properties and multiple possible applications overviewed by *E.* Lassner and W.D. Schubert [1]. Tungsten is known having the highest melting point of all metals, T_m = 3411 ± 28°C. The macrohardness for polycrystalline tungsten can be up to 650 Vickers with Young's modulus, E = 390–410 GPa. The room-temperature ultimate tensile strength (UTS) of polycrystalline tungsten rods is commonly in the range of 580–1470 MPa. Strength, plastic and creep properties of tungsten are of paramount interest for its widespread use as a structural material. The hot strength of pure tungsten is exceeded only by that of rhenium. Alloys based on W-Re-HfC are the strongest man-made metallic materials produced at temperatures up to 2700 K. Doped tungsten wires are the most creep-resistant wires, with the exception of monocrystalline tungsten [1].

Unfortunately, the electrodeposition of pure tungsten deposits from aqueous tungstate solutions is not viable and possibly hindered by the formation of an oxide layer on the cathode during electrodeposition. That oxide cannot be directly reduced to metallic tungsten, due to a very low overvoltage for hydrogen evolution on tungsten [1]. However, tungsten can be easily codeposited with iron group metals, and publications dealing with electrodeposition of tungsten alloys with iron-group metals can be found as early as in the 1930s [2–4]. The first commercial Co-W alloy electrodeposition process was reported by Schwartz [5], indicating the role of citrate species as an important factor to achieve the desirable morphology and structure of deposits. It was also shown that the cathode current efficiency was less than 100 %, which suggested that the hydrogen discharge reaction possibly contributes to the process.

Early theoretical studies on W (and Mo) codeposition with iron group metals were initiated by Brenner [6], Holt and Vaaler [7, 8], Fukushima [9] and Vasko [10]. According to Brenner [11], tungsten codeposition with iron group metals – Me (*i.e.,* Ni, Fe, Co) from aqueous electrolytes is called “induced codeposition”. Citrate complexes were identified by Bobletsky and Jordan [12, 13] and later used to explain the species involved in the electrodeposition of W (Mo) alloys by Holt and co-workers [14, 15]. Other types of electrolytes have also been found useful for tungsten alloys electrodeposition, namely: malic, tartaric, gluconic, glucaric [16–19], acetic [20], glycine [21–24] and pyrophosphates [24].

Theoretical and practical studies of tungsten alloys with iron group metals (Me-W) continue to be carried out worldwide, in the light of versatile applications of these alloys due to their specific mechanical, tribological, magnetic, electrical and electro-erosion properties as well as corrosion resistance. Fig. 1 captures this growing interest in this area as the number of scientific papers published in the top-rated journals. Me-W alloys may compete even with ceramics and graphite by virtue of their high thermal resistance. Furthermore, tungsten alloys with a nanocrystalline microstructure make up mechanically hard coatings that have favorable wear and anti-corrosion properties, which make them extremely attractive for replacing hard Cr coatings in many applications where aggressive conditions exist [18]. That includes processes where lubrication or dry friction conditions take place, for example in hydraulic equipment, as well as those where a lubricant may be difficult to maintain, for ex., in aerospace drives and splines where low friction in dry conditions over a limited period of flight may be a valuable asset [18]. Tungsten alloys can also be used as a barrier layer for ultra large-scale integration devices (ULSI) [26] and micro-electro-mechanical systems (MEMS) structures [26, 27], then, as catalysts for clean hydrogen generation from water splitting [28]. It is worth noting that Me-W show also a tunable magnetic behavior, ranging from soft or semi-hard ferromagnetic properties (for moderate W contents) to non-ferromagnetic, when the W content exceeds 25–30 at.% [29].

The aim of the present paper is to provide an overview of the researches on electrodeposition of tungsten alloys with iron group metals, their properties and applications.

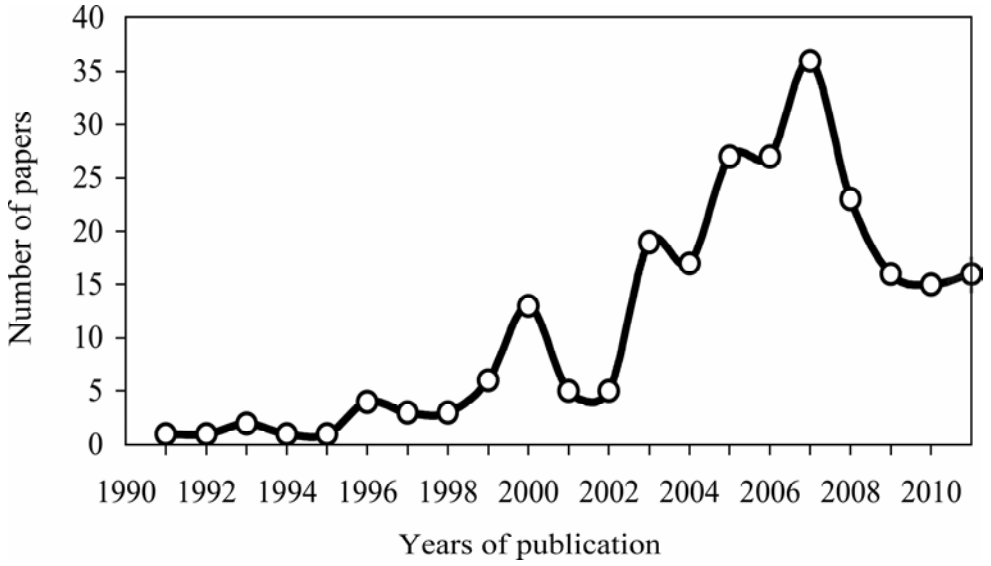

Fig. 1. Number of papers on theoretical and practical aspects of W alloys electrodeposition published in the issues referred by "ISI Web of Knowledge" database (WEB of Science® and Science Citation Index Expanded™).

CHEMISTRY OF ELECTROLYTES USED FOR W-ALLOYS ELECTRODEPOSITION

Understanding the chemistry of the electrolytes used for alloy electrodeposition is important to unveil the factors controlling the performance of the plating bath and the peculiarities of codeposition of alloy constituents.

Any practical use of electrolytes containing only iron-group metal salts (*i.e.*,"simple" baths with *e.g.,* sulphates, chlorides) and WO_4^{2-} without ligands is limited due to the formation of sparingly soluble hydroxides and tungstates of corresponding iron-group metals (Me – Co, Ni and Fe); these hydroxides precipitate at pH>7.5–7.7 [30], and the iron-group tungstates precipitate at pH>2–3 [31–33].

A number of different W(VI) polynuclear species are present in water when tungstates are dissolved depending on the pH values:

- at pH > 7.8 WO_4^{2-} ion is the predominant species in solution, whereas $W_{12}O_{42}^{12-}$ is the main species at pH<7.8, and it is in a protonated form at pH<5.7 [34]. Also, $W_7O_{24}^{6-}$ (paratungstate-A) and $H_2W_{12}O_{42}^{10-}$ (paratungstate-B) can exist [35].
- at pH<5 equilibria are slowly established and $W_{12}O_{41}^{10-}$ and $HW_6O_{21}^{5-}$ are dominating [35–36];
- at pH 4 $HW_6O_{21}^{5-}$ protonates into $H_3W_6O_{21}^{3-}$ which with time forms the stable metatungstate ion $[H_2(W_3O_{10})_4]^{6-}$ [37];
- at pH 1 the main tungsten species in solution is the hydrated tungstic acid $WO_3 \cdot 2H_2O$ [38].

In Fig. 2 we provide the calculated mole fractions of W(VI)-containing species vs. pH in a solution containing 0.1 M Na_2WO_4. The calculation is based on the available equilibrium constants including tungstic acid and tungstates [36, 39]. The amount of "free" WO_4^{2-} is reduced sufficiently at pH<5 and at pH 2–3 the concentration of WO_4^{2-} decreases down to 10^{-10} M due to the formation of $W_{12}O_{39}^{6-}$ species. However, if an iron-group metal is added as a sulfate salt, the ion- pairing (or ion-associates) Me^{2+}:SO_4^{2-} will dominate, which is not the case in chloride or nitrate solutions. This reduces the concentration of "free" Me^{2+}-ions down to 10^{-3} M or even below in a 0.2 M $MeSO_4$ solution [40]. Therefore, solutions containing Na_2WO_4 and $MeSO_4$ are stable at pH<3 because of the $MeWO_4$ solubility product K_{sp}: *e.g.* $K_{sp} = 10^{-13}$ for $FeWO_4$ [41]. Such solutions can be used to obtain W-containing alloys, *e.g*., Fe-W [42–43] or Co-P-W [44]. When pH rises to 3–6, the concentration of "free" WO_4^{2-} ions increases up to 10^{-7}–10^{-5} M, which is high enough to exceed the solubility product, K_{sp}, of $MeWO_4$, and therefore insoluble $MeWO_4$ are formed and precipitate in the absence of complexing ligands.

Complexing is used as a method to approach the electrode potentials of different metals by reducing the concentration of "free"Me^{2+} ions and increasing the solubility of Me(II) salts in baths containing OH^-, $WO_4^{2-}$and PO_4^{3-} [44, 45]. Several common electrolytes are known and used for the electrodeposition of tungsten alloys with iron-group metals but the number of complexing agents used is limited (citrates, pyrophosphates [23, 24], tartarates [16, 17], gluconates [18, 19]). Usually, a certain formulation can be adapted for the codeposition of Co, Ni and Fe alloys with W, as well as for the electrodeposition of ternary alloys [40, 46–49] by simple exchange of iron group metals salts. When citrates or pyrophosphates are using as complexing agents, the concentrations of Co^{2+} and Ni^{2+} in solution decrease 10^4–10^6 times compared to those in ligand-free solutions [40, 50]. The added citrate modifies the distribution of tungsten-containing species, and various complexes of the type $[(WO_4)_p(HCit)_qH_r]^{(2p+3q-r)-}$ are formed. The stability constants of eight tungstate-citrate complexes are provided in [51].

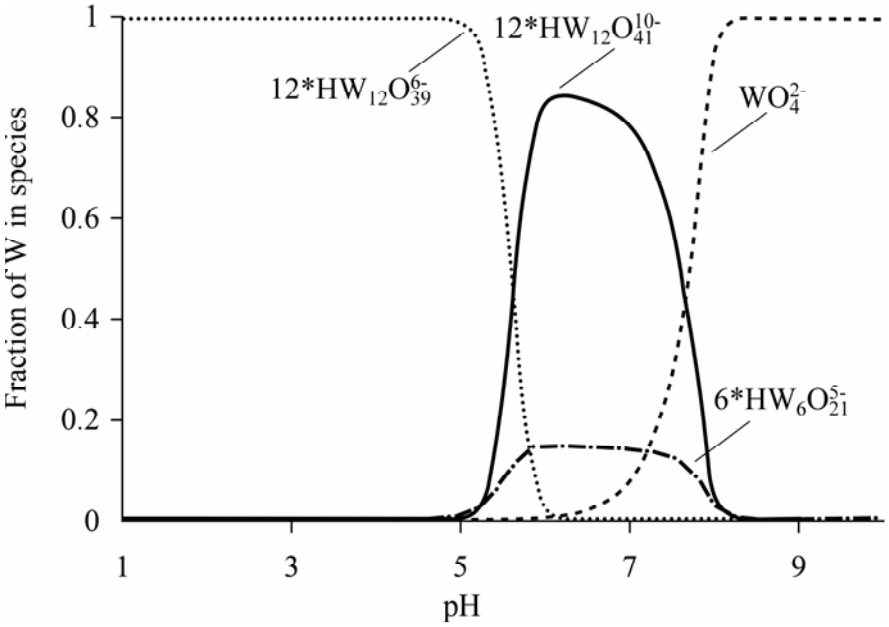

Fig. 2. Mole fraction of tungsten species in a 0.1 M Na_2WO_4 solution.

In Fig. 3 we show the calculated mole fractions of tungsten species in an equimolar tungstate-citrate solution vs. pH. Under these conditions at low pH, only one polytungstate complex, $W_{12}O_{39}^{6-}$, is formed in sufficiently high amounts. In the entire range of pH values, different tungstate-citrate complexes are formed and the main ones are the following:

- $[(WO_4)_1(HCit)_1H_3]^{2-}$, $[(WO_4)_2(HCit)_2H_5]^{5-}$ and $[(WO_4)_2(HCit)_1H_4]^{3-}$ at pH 2–4,
- $[(WO_4)_2(HCit)_2H_6]^{2-}$ and $[(WO_4)_1(HCit)_1H_2]^{3-}$ at pH 4.5–7.5;
- $[(WO_4)_1(HCit)_1H_4]^{4-}$ at pH 7–9.

Only at pH>9, the WO_4^{2-} species becomes predominant. A similar distribution of tungsten-containing species should remain also in the citrates-containing solutions for tungsten alloys electrodeposition, where the concentrations of iron-group metals are relatively low in comparison with those of citrates; and simultaneously, the concentrations of citrates are compatible with those of tungstate, *e.g*, for Ni-W [46, 47, 52–56], Co-W [46, 57–59], Fe-W [46, 60, 61], and ternary alloys [47, 49].

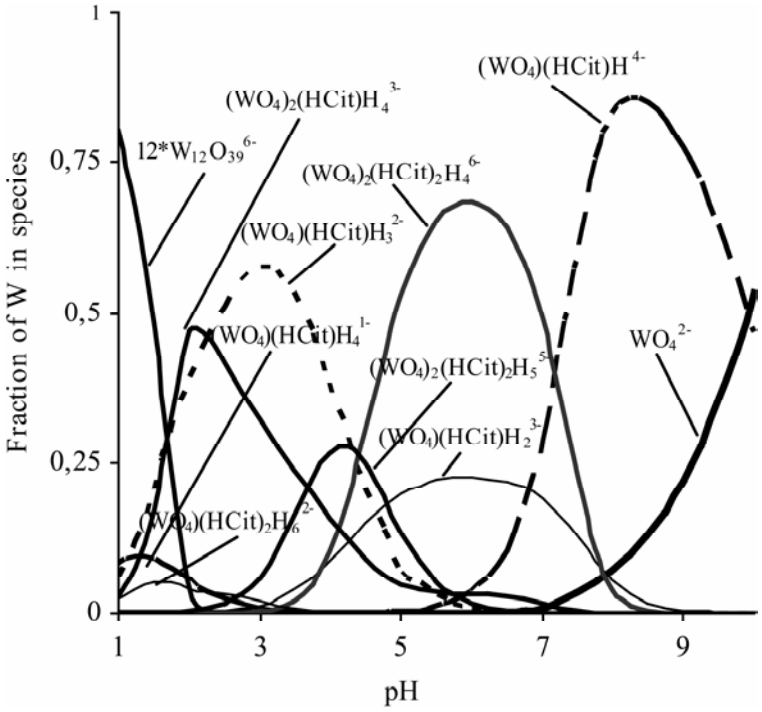

Fig. 3. Mole fraction of tungsten species in solution with equimolar quantities of Na_2WO_4 and citrate.

The content of Me and W in the alloy depends on the ratio of the partial current densities (PCD) for tungsten and Me. Moreover, the PCD for tungsten can correlate with the PCD of the iron-group metal [62]. When the WO_4^{2-} concentration in solution is higher than the Me salt concentration, the PCD for W is the highest under such conditions and, therefore, deposits with relatively high W contents are obtained, irrespective of the total current applied, *e.g.*, at least 20–25 at.% W for Ni-W, and 30–35 at.% W for Co-W and Fe-W alloys. However, the Faradaic efficiency (FE) is relatively low and in most cases does not exceed 10–15%.

In order to increase both the FE and deposition rate, solutions containing higher concentrations of the iron-group metals salts (0.1–0.2 M) are used whereas the concentration of citrates is kept at the level of 0.3–0.5 M [44, 45, 63–66]. This brings about an increase in the FE up to 30% for Fe-W, up to 33–50% for Ni-W, and 60% for Co-W. Under these conditions, the distribution of species in solution differs from the one presented in Fig. 3. Citrate complexes both with tungstate and iron group metals are leaving a sufficient fraction of "free" Me^{2+} ions (at pH<3–4) or ionic pairs "Me^{2+}:SO_4^{2-}" (at pH<7–8) in solution. As an example, the calculated mole fractions of tungsten (VI) and Co(II) species are provided in Figs. 4,*a-c*. For the Ni-W case, the calculated distributions of W(VI) and Ni(II) are similar to those for Co(II). In these solutions low soluble tungstates of iron-group metals are not formed within the entire range of the working pH due to either low WO_4^{2-} concentrations at a low pH or low Me^{2+} ions concentrations at a higher pH. The increase in WO_4^{2-} concentration with the solution pH (Fig. 4,*c*) correlates with the increase in W content in the alloys deposited at the same fixed overall current density at pH ranged from at least 5 to 8.5 [45, 64, 67–69]. Indeed, the dependence of W content in alloys vs. pH at the same total current density has the maximum at pH 8–8.5, that cannot be predicted based on the increasing of [WO_4^{2-}] with pH (Fig. 3) at pH<6.5 or the plateau in [WO_4^{2-}] at pH>6.5 (Fig. 4,*c*). It can be supposed that WO_4^{2-} ions might form other complexes at a higher pH. Thus, the codeposition data were analyzed by assuming the formation of a mixed complex $[(Ni)(WO_4)(Cit)(H)]^{2-}$ in solution [70, 71]. Also, the formation in an electrolyte that contains citrate complexes of cobalt and tungsten may include the formation of compounds with enhanced molecular mass, probably polynuclear heterometallic complexes containing an iron-group metal (*e.g.* Co) and W(VI), as discussed in [72]. However, the stability constants of these heteronuclear complexes are not presented in this reference. In addition, the slow adsorption stages occurring on the surface during both pure iron-group metal [73] and alloys with W alloy electrodeposition [74] hinders an accurate prediction of tungsten content as a function of pH.

Ammonia (NH_3) is frequently added to plating baths to fine-tune the pH within the range of 7.0–9.0 and to increase the FE, especially in the case of Ni and Fe alloys electrodeposition. In the case of Co alloys, the distribution of Co(II) complexes in solution with or without NH_3 is almost the same, so that little effect is impaired on the FE of Co-W [40, 50]. Nevertheless, ammonia plays a key role in the baths, namely as a buffering agent. The composition of W-containing electrodeposited alloys is very sensitive to the solution pH

[67, 69, 75, 76]. In the case of W alloy electrodeposition, the electroreduction of WO_4^{2-}-ion and hydrogen evolution reactions are associated with increasing pH at the electrode surface, which yields the electrolyte alkalization in the boundary layer near the electrode that can sufficiently increase or decrease the W content in the alloys, depending on the initial pH. A constant alloy composition along the entire thickness of electrodeposits can be achieved if the OH^- ions released during the electroreduction of tungstate further participate in the fast acid-base equilibrium reactions with hydrogen ions, keeping the pH in the near electrode layer almost constant. In other words, the electrolyte must possess a high buffer capacity; otherwise, compositionally graded deposits would be expected. The buffer capacity as a function of pH in the citrate-ammonia system was analyzed in [44, 45, 67]. It was shown that at pH<7.5 the buffer capacity is controlled by the concentration of citrates. Therefore, for the electrodeposition of W alloys from acidic solutions it is unnecessary to use ammonium salts as buffering additives. Usually the electrodeposition of W alloys is carried out at elevated temperatures. For the ammonia concentration of 0.8 M, the minimum buffer capacity at 70°C is not as deep as at room temperature.

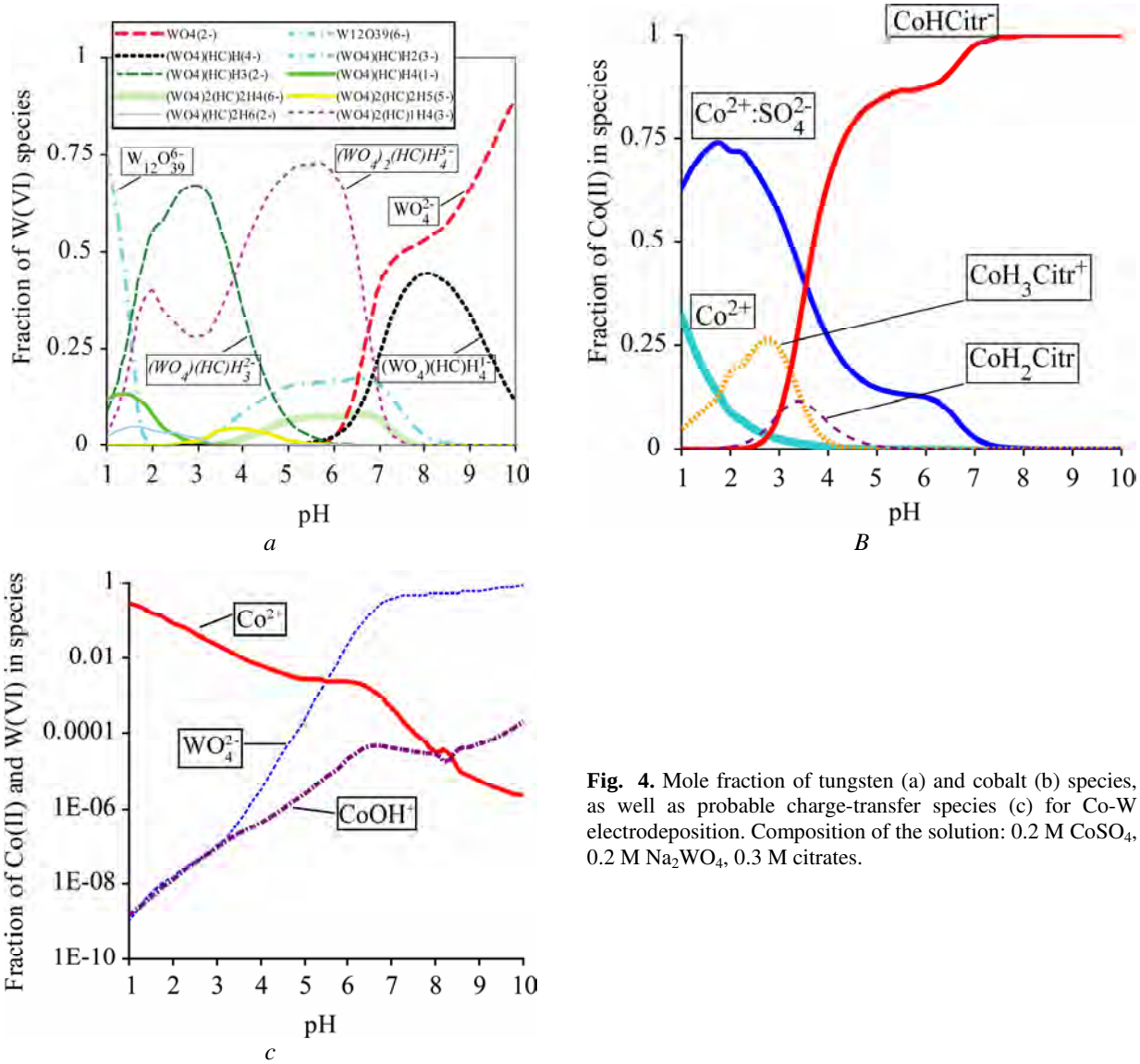

Fig. 4. Mole fraction of tungsten (a) and cobalt (b) species, as well as probable charge-transfer species (c) for Co-W electrodeposition. Composition of the solution: 0.2 M $CoSO_4$, 0.2 M Na_2WO_4, 0.3 M citrates.

The maximum in buffer capacity shifts to lower pH values if the electrolyte temperature is increased. For example, deposition at near room temperature and at pH of 8.5 would not be a good choice, whilst at 70°C the deposition works fine. In order to reduce possible evaporation of ammonia from the electrolytes during long-term electrolysis at elevated temperatures and thus to keep the alloy deposition rate stable and offset the increase in pH values due to the reduction of WO_4^{2-} and the hydrogen evolution, it is recommended to perform electrodeposition at pH values as low as possible (7.5–8.0). In this case, a sufficient fraction of the ammonia added to the solutions transforms into the non-volatile NH_4^+-ionic form. Moreover, because of better buffering properties of solutions at these pH values, a higher concentration (1.5 M) of ammonia is recommended as well [45, 67]. The electrodeposition from aqueous baths is generally carried out in non-

hermetic cells. In this case, however, significant amounts of ammonia could evaporate during long-term electrodeposition at elevated temperatures, which results in a decrease of both pH and deposition rate. In order to avoid the decrease in pH due to ammonia evaporation, Na_2CO_3 can be introduced additionally to the electrolyte to maintain the desired pH. In the absence of Na_2CO_3, the amount of W in the Ni-W alloys is more sensitive to pH than to the current density, and there is a large difference in deposit composition at pH between 8.5 and 10. Therefore, adding Na_2CO_3 to the bath reduces the effect of both pH and the current density on W amount in the Ni-W alloys [45].

As the presence of NH_3 is not critical for Co-W alloys electrodeposition, boric acid is added to the solution for buffering purposes instead of ammonia, so this solution does not contain volatile components [63]. In this solution, the buffer capacity remains almost constant at the level of 0.2–0.4 mol/l in the range of pH 6 to 11. Whereas at 70°C, the buffer capacity in the narrower pH range, i.e. from 7 to 9 is even higher than or the same as that was obtained at lower temperatures [64].

Generally, the chemical composition of the electrodepositing alloy depends on the ratio of the PCD for alloy's constituents. However, the value of the PCD is influenced by a number of factors such as chemistry of solution, total current density applied, temperature, hydrodynamics, etc. Therefore, at a given pH, the increase of overall current density may result either in a decrease [68, 77], increase [18, 19, 64] in the tungsten content in the alloys, or it can remain almost constant [65, 67].

CODEPOSITION MECHANISMS

The deposit composition of alloy resulting from an electrodeposition process is a key parameter for the design of requisite material properties, and is a direct consequence of the ratio of metal species reduction reaction rates (*i.e*., partial current densities) that occur. Understanding the phenomena that determine the PCD is thus essential to be able to predict and control the deposition. The induced codeposition behavior of tungsten alloy electrodeposits from aqueous media introduce a further complexity in that both kinetic and transport mechanisms can be coupled. In this section, the kinetic mechanisms and the coupled nature of mass transport effects are discussed.

One of the earliest reports to describe the kinetic mechanism of tungsten codeposition with iron-group element was made by Holt and Vaaler [8]. A "catalytic reduction" theory was proposed to explain the reduction of aqueous tungstate solutions in the presence of the zero valence state of an iron-group element, Me (i.e., Ni, Co and Fe). The following two cathode reactions are suggested as being essential to the reduction process:

$$Me^{2+} + 2e^- \rightarrow Me, \tag{1}$$

$$WO_4^{2-} + 8H^+ + 6e^- \xrightarrow{Me} W + 4H_2O. \tag{2}$$

The iron-group element reduction occurs first, which then catalyzes tungsten deposition, until the surface is replete with tungsten, arresting the tungsten deposition. This proceeds until a new layer of the iron-group element is formed. The observation of laminated structures germinated this concept, although as stated by Younes and Gileadi [78], non-laminated, solid solution alloys of tungsten with iron-group elements can also be readily electrodeposited. That seminal work [8] was also reviewed by Vasko [10]. He pointed out that while metals of the iron-group are active catalysts, it is also known that W can co-deposit on other, very inactive metals (*e.g.*, Mn, Sb, Cu and Sn) but to a small extent. Another important implication of the assumption that the solid phase of an iron-group metal acts as a catalyst, is that the amount of W that can be theoretically codeposited into an alloy is restricted to an inherent upper limit. A review of earlier works in [10] provides these upper W wt % limits: 53 wt % with Ni, 65 wt % with Co, and 80 wt % with Fe.

While Holt and Vaaler [8] did recognize that tungsten codeposition occurs with Faradaic efficiencies less than 100%, due to the hydrogen evolution side reaction, they did not place a direct dependence of hydrogen on the tungsten mechanism. In contrast, Clark and Lietzke [79], emphasizing the role of hydrogen, presented a different mechanism where, first, there was a deposition of a partially reduced tungstate film on the cathode, followed by the catalytic reduction of this film by hydrogen in the presence of freshly deposited iron, cobalt, or nickel. Without the inducing element, the tungstate ion is just partially reduced, and due to its low overpotentials to hydrogen evolution, cannot reduce further. They also stated that the reacting species were those that were complexed and did not rule out iron, cobalt or nickel tungstate species.

Iron-group metal tungstate complexes that are precursors to tungsten alloys is a concept introduced by Younes and Gileadi [78], Younes-Metzler *et al.* [70], and reviewed by Eliaz and Gileadi in [80]. The idea of implicating the mixed-metal soluble complexes as a prerequisite for iron-group and tungsten codeposition was motivated by the observation that the partial current density of Ni depends on the amount of tungstate in

the electrolyte and vice versa. In publications on Ni-W codeposition, Gileadi et al proposed a complex composed of Ni^{2+}, WO_4^{2-} and deprotonated citrate. While it was recognized that bimetallic complexes can exist with citrate, none has been identified with an iron-group metal and tungsten. Soluble complexed species as the means for codeposition of Co and W has also been suggested by Aravinda *et al.* [81]. They identified a cobalt citrate complex with UV absorption studies, but not a mixed-metal complex, and to explain shifts in cyclic voltammetry curves, they postulated that alloy deposition is possibly from a cobalt-tungstate complex. A gluconate (gluc) containing electrolyte for Co-W depostion was examined by Weston *et al.* [18] with UV spectroscopy and by comparing spectra with different amounts of added species they deduce that significant quantities of a mixed metal complex occurs, [Co–gluc–WO_4^{2-}]. They observed a decrease in the reduction current density with an increase in the quantity of the ternary mixed-metal complex and concluded that this one may be more difficult to reduce than a binary complex. They attributed the high W content in the deposit directly from the reduction of a ternary complex, consistent with Younes and Gileadi [78], and Eliaz and Gileadi [80] points of view. In addition, Belevskii *et al.* [82] detected a heteropolynuclear Co–W citrate complex through the evaluation of gel chromatography.

However, the formation of various complexes does not explain the variety in dependencies of W content in the alloys on the electrodeposition conditions. The Vasko film model reviewed in [10, 11] is an alternate interpretation. For instance, when employing Ni-W, the formation of a nickel hydroxyl species, $NiOH^+$, $NiOH_{ads}$ aids the adsorption of tungstate species:

$$Ni^{2+} + OH^- \leftrightarrow NiOH^+, \tag{3}$$

$$NiOH^+ + e^- \leftrightarrow NiOH_{ads}, \tag{4}$$

$$nWO_4^{2-} \leftrightarrow \left(W_f O_g^{y-}\right)_{ads}. \tag{5}$$

A heteropolytungstate film is formed with a certain composition that is not defined, $[H_pNi_qW_rO_s]_w$ giving the following overall, two-step reaction:

$$NiOH^+ + 3H_3O^+ + WO_4^{2-} \leftrightarrow \left[H_pNi_qW_rO_5\right]_w, \tag{6}$$

$$\left[H_pNi_qW_rO_5\right]_w + ne^- \rightarrow Ni - W + mO^{2-} + nOH^-. \tag{7}$$

The ensuing high resistance in the cathode surface creates a high negative potential at the metal (alloy)–film interface. The heteropolytungstate film is gradually reduced to the alloy and at the same time new layers of the film are continuously formed. Since films were not always observed during deposition, this model has lacked popularity. However, recently, Juškėnas *et al*. [84] reported a transient in the Ni-W composition during film growth that was mapped by in situ X-ray diffraction (XRD). They state that the Vasko model fits these best, and has renewed interest in this concept.

The induced codeposition behavior of tungsten alloy reduction has often been considered similar to molybdenum alloy reduction and analogies of mechanisms from molybdenum studies warrants discussion. Early Ni-Mo electrodeposition was also studied by some of the same authors. Ernst *et al*. [14], and Ernst and Holt [15] proposed that the induced elements, Mo or W, formed a mixed oxide intermediate at the electrode surface which was subsequently reduced by hydrogen to solid metal. This approach stems from the observation that generally as more Mo (or W) is codeposited into an alloy the hydrogen side reaction tends to be higher, or in other words, the current efficiency is lower. The mechanism was expanded by Fukushima *et al*. [85] assuming that hydrogen was adsorbed onto the codeposited iron-group element and that the inducing element was reduced at these sites. This assumes that the solid iron-group metal acts as a catalyst in reducing Mo and that a theoretical upper limit exists for Mo codeposited in an alloy. More recently, this group [86] suggested that the electrodeposition behavior of W-iron-group metal alloys can be explained by the reduction mechanism with atomic hydrogen similar to the induced codeposition of Mo. An earlier work showed that the adsorbed hydrogen onto the reduced iron-group metal, H(Me), induces the reduction of the molybdenum oxide intermediate [18].

$$Me^{2+} + 2e^- \rightarrow Me, \tag{8}$$

$$H^+ + e^- \xrightarrow{Me} H(Me). \tag{9}$$

$$MoO_4^{2-} + (6-n)e^- \rightarrow Mo^{n+}\text{oxide(hydroxide)}, \tag{10}$$

$$Mo^{n+}\text{oxide(hydroxide)} + n\text{H(Me)} \rightarrow \text{Mo(Me)}. \tag{11}$$

Assuming a tungsten oxide intermediate with a +4 valence state, four hydrogen atoms are needed to reduce a W(IV) oxide to a W atom and every Ni atom can adsorb 0.6 hydrogen atoms, which is equal to the number of unpaired 3d electrons in Ni. Thus, when the atomic hydrogen bonds to the Ni atom, this contributes to the reduction of the W(IV) intermediate the ratio of W atoms to Ni is 0.6/4 (32 wt %). A higher amount of W(IV) oxide intermediate forms when more tungstate is in the solution and to reduce this the Ni atoms have to contribute to the reduction several times. Oue *et al*. [86] found by x-ray photoelectron spectroscopy (XPS) that unreduced tungsten oxide accompanied solid W at high tungstate electrolyte concentrations and that the Ni(II) reduction rate was simultaneously inhibited, and in turn decreased the reduction rate of tungsten. The deposited Ni-W alloys had two distinct regions, depending on the relationship between the alloy composition and the current efficiency: a region of a low W content in the deposits, where the partial current efficiency for W deposition increases with the W content, and a region of a high W content in the deposits, where the partial current efficiency of W decreases with an increase in W content.

Chassaing *et al*. [87] suggested that the iron-group ion was responsible for the formation of the intermediate, not the solid state, and that the intermediate was reduced by hydrogen forming solid Ni and Mo, codeposited as an alloy. At low overpotentials, where only an oxide was formed, Auger electron spectroscopy (AES) and energy dispersive x-ray spectroscopy (EDS) identified a molybdenum-nickel oxide intermediate having a 4:1 ratio of Ni to Mo. They suggested the following induced codeposition mechanism: when no alloy deposit is formed, the following two reactions occur:

$$MoO_4^{2-} + 2H_2O + 2e^- \rightarrow MoO_2 + 4OH^-, \tag{12}$$

$$MoO_2 + 4Ni^{2+} + 8e^- \rightarrow MoO_2Ni_4. \tag{13}$$

at larger overpotentials, when an alloy deposit is formed, then the overall reaction proceeds as:

$$MoO_4^{2-} + 3Ni^{2+} + (4-n)H + 8e^- \rightarrow MoNi_3 + 4OH^- + nH \tag{14}$$

with a mixed-metal intermediate.

More recently, Gómez *et al.*[88] showed that the first stage of the alloy formation involved partial reduction of Mo to different oxidation states consistent with that reported by Fukushima *et al*.[86] and, Chassaing *et al.*[87] In both the Fukushima and Chassaing models there is an upper limit for Mo (or W) codeposition in an alloy. To date, the highest amount of W codeposited with Ni is 50–67 a/o (76–86 w/o) W in a Ni-W alloy, as reported by Younes and Gileadi [78], and the highest amount of Mo codeposited with Ni is 50–74 a/o (62–82 w/o), as reported by Sun and Podlaha [89], although both with impractically low Faradaic current efficiency.

While it was possible to find deposition conditions where an increase in Mo concentration in the deposit was accompanied by a drop in the current efficiency and thus hydrogen evolution, it was also possible to find the contrary situation, calling into question the decisive role of hydrogen [90]. A different modeling approach was proposed by Podlaha and Landolt [91, 92], which explained the induced codeposition of Mo (or W) via a catalysis reaction, assuming the catalyst was a mixed Mo (or W)-iron-group intermediate, but without the need for the adsorbed hydrogen. The mixed-metal intermediate could adsorb at the electrode surface and was subsequently reduced without any controlling feature being dominated by the hydrogen evolution side reaction. The mechanism was initially reported for Ni-Mo electrodeposition [15] from a citrate electrolyte, and then generalized to other codepositing iron-group elements (Fe, Co) [92]; assuming a complexed nickel ion species with a citrate ligand, $NiCit^-$, which was not intended to capture the details of complexation, the mechanism was presented as:

$$NiCit^- + 2e^- \rightarrow Ni(s) + Cit^-, \tag{15}$$

$$MoO_4^{2-} + NiCit^- + 2H_2O + 2e^- \rightarrow [NiCitMoO_2]^-_{ads} + 4OH^-, \tag{16}$$

$$[NiCitMoO_2]^-_{ads} + 2H_2O + 4e^- \rightarrow Mo(s) + NiCit^- + 4OH^-. \tag{17}$$

where Cit^- represents $[C_6H_5O_7]^{3-}$, and while the $NiCit^-$ species is to represent the complexation of Ni(II) with a citrate species, the exact form of the species will, of course, depend upon the electrolyte composition and pH. That mechanism should be viewed as being cognizant of complexing equilibria without specific details. Similarly, the Ni species could also be replaced with Co or Fe. The molybdate species in the above mechanism could be equally replaced with tungstate species to make this model more general. If assuming that the iron-group species acts as a catalyst, and that it is reduced independently to the mixed-metal ion intermediate, then no limitation is placed on the quantity of Mo (or W) that can be codeposited. Gómez *et al.* [88] took this mechanism one step further and suggested that the $NiCit^-$ complex species catalyzes the molybdenum oxide that is initially formed, combining the features of the Chassaing and Podlaha-Landolt models. With this assumption, when there is no $NiCit^-$ present in the electrolyte, the partially reduced molybdenum oxides are predicted.

The Podlaha–Landolt model does exclude the importance of the side reaction and confirmes that, indeed, the adsorbed intermediates of hydrogen can also compete with the mixed-metal intermediates, indirectly influencing the reaction rate. For example, when molybdenum or tungsten alloys are tested for catalyzing hydrogen evolution, the Tafel slopes can be related to conventional hydrogen evolution kinetics; Jakŝić [93] noted that on NiMo alloys hydrogen evolution follows the Volmer-Heyrovsky mechanism in base electrolytes, with a high surface coverage by the adsorbed hydrogen, according to:

$$H_2O + e^- \leftrightarrow H_{ads} + OH^-, \tag{18}$$

$$H_{ads} + H_2O + e^- \rightarrow H_2 + OH^-. \tag{19}$$

If assuming a similar mechanism occurring during deposition of the alloy, then the adsorbed hydrogen may be significant enough to affect the available free surface sites for the Mo (or W) and the iron-group intermediates. In a similar manner, the deposition of the iron-group elements can also occur with coverage of an adsorbed intermediate. For example, Ni, Fe and Co elemental electrodeposits have been widely modeled via an adsorption intermediate [94–100]:

$$Me(II) + e^- \rightarrow [Me(I)]_{ads}, \tag{20}$$

$$[Me(I)]_{ads} + e^- \rightarrow Me(s). \tag{21}$$

and, hence, can also alter the free electrode surface area available for the Mo (or W) reduction reaction.

The utility of the Podlaha-Landolt model is best shown in the coupling of the kinetic and transport regimes of the molybdenum reduction reaction (see Fig. 5). When the concentrations of the inducing iron group ions (*e.g.*, Ni) in the solution are very low compared to those of molybdate (or tungstate), then the Mo (or W) reduction would be limited by the amount of available inducing ions. In addition, species that are in low concentrations quickly reach their mass transport limit (i.e., limiting current density). Thus, in uncoupled reactions, if one metal ion species is in excess, and another species is, in contrast, having a very low concentration in the electrolyte, it is possible to electrodeposit in the regime where the species in excess exhibit a kinetic control and the other exercises a mass transport control during codeposition. In this case, an increase in the electrolyte agitation will increase the amount of the minor species in the deposit due to its increased limiting current density (Fig. 5,*a*). However, the induced codeposition behavior does not mirror this expectation. If the minor species in the electrolyte are any of the inducing elements (*e.g.*, Ni, Fe or Co) and if it is under mass transport control, then with an increase in the electrode or electrolyte agitation, its partial current density will increase and so will the reluctant metal (Mo or W) reaction rate, keeping the deposit concentation relatively insensitive to agitation (Fig. 5,*b*). Or said another way, the inducing element appears to be transport controlled even though its concentration in the electrolyte is in excess and is unexpectedly influenced by such transport factors as changes in the hydrodynamic environment. The opposite scenario, when the reluctant element, such as the tunsgtate species is the minor component, it behaves as expected under transport control with an increase in its PCD, as though it is apparently decoupled as long as an iron-group element is codepositing (Fig. 5,*c*).

To capture this effect, a steady-state model that integrates both transport and kinetics in needed. An example is given in Table 1, that follows the second model presented by Podlaha and Landolt [92], where the fractional adsorption of the reacting complexed iron-group metal, θ_{ML}, was included along with the adsorption of the mixed-metal molybdate intermediate, $\theta_{Mo\text{-}ML}$. The reduction reaction rates for the inducing element was assumed to be governed by the Tafel kinetics, and a Nernstian boundary layer approach was

adopted where diffusion dominates within the boundary layer, and the boundary layer size, δ, is established by convection induced by the hydrodynamic environment near the electrode surface from electrode or electrolyte agitation.

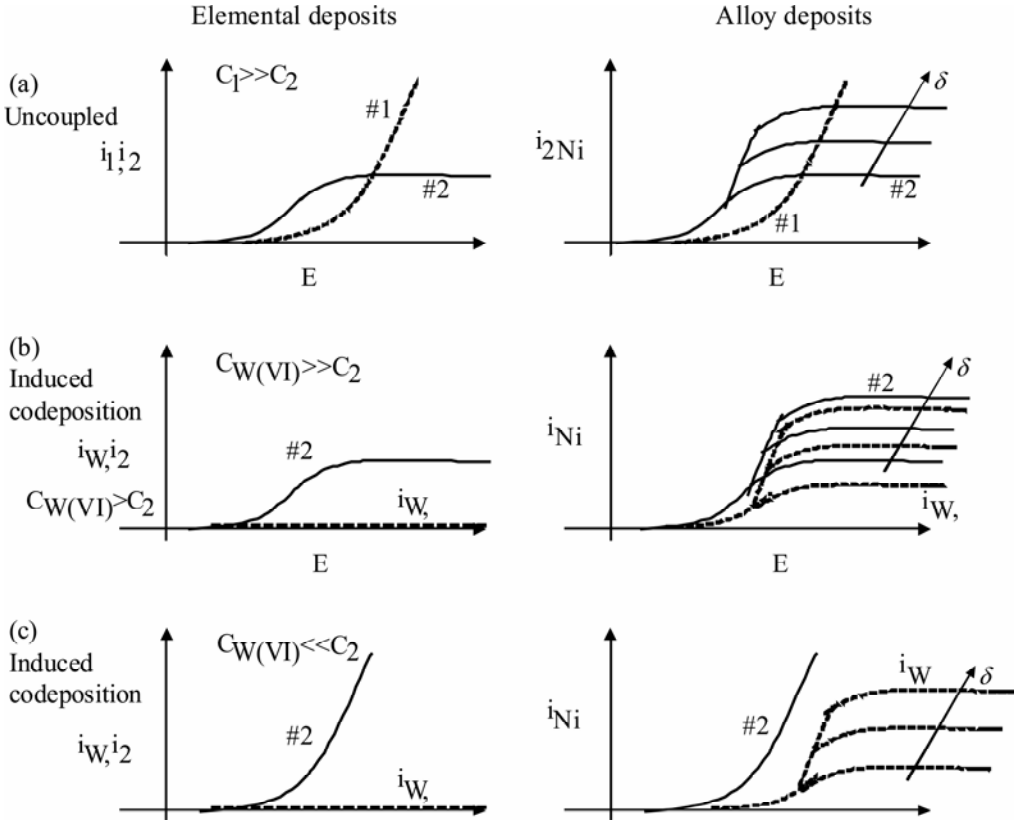

Fig. 5. Comparison of PCD in a kinetically, uncoupled (a) versus induced codeposition (b) behavior alloy reduction when one species, #2, is reduced under mass transport control. A change in the boundary layer thickness alters only species #2 in an uncoupled alloy codeposition, while it affects both species #2 and the inducing element, *e.g.*, W.

Table 1. Summary of the Podlaha-Landolt model of induced codeposition [92]

Boundary conditions at the electrode	Governing equations	Boundary conditions at the boundary layer thickness, δ
$N_{ML} = \frac{i_{ML,1}}{F} + \frac{i_{Mo,1}}{4F} - \frac{i_{Mo,2}}{F}$ $N_{MoO_4^{2-}} = \frac{i_{Mo,1}}{4F}$ $\frac{i_{ML,1}}{F} = -k_{c,ML,1} C_{ML}^s \left(1-\theta_{ML}-\theta_{Mo\text{-}ML}\right) e^{\left\{-\frac{\alpha_{c,ML,1} F}{RT} E\right\}}$ $\frac{i_{ML,2}}{F} = -k_{c,ML,2} \theta_{ML} e^{\left\{-\frac{\alpha_{c,ML,2} F}{RT} E\right\}}$ $\frac{i_{Mo,1}}{2F} = -k_{c,Mo,1} C_{ML}^s C_{MoO_4^{2-}}^s \left(1-\theta_{ML}-\theta_{Mo\text{-}ML}\right) \theta_{ML} e^{\left\{-\frac{\alpha_{c,Mo,1} 2F}{RT} E\right\}}$ $\frac{i_{Mo,2}}{4F} = -k_{c,Mo,2} \theta_{Mo\text{-}ML} e^{\left\{-\frac{\alpha_{c,Mo,2} 4F}{RT} E\right\}}$ $\frac{i_{side}}{F} = -k_{c,side} C_{ML}^s \left(1-\theta_{ML}-\theta_{Mo\text{-}ML}\right) \theta_{ML} e^{\left\{-\frac{\alpha_{c,side} F}{RT} E\right\}}$	$\nabla \cdot N_{ML} = 0$ $\nabla \cdot N_{MoO_4^{2-}} = 0$ assuming a Nernstian approach : $N = -D\frac{dC}{dx}$ for each species	$C_j = C_j^b$

Fig. 6 illustrates the transport influence when Ni ions are in low concentration compared to molybdate codeposited onto a rotating cylinder electrode, $C_{Ni(II)} << C_{Mo(VI)}$, hence the boundary layer can be defined by $\delta = 99.62 d_i^{-0.4} \nu^{0.344} D_{lim}^{0.356} S^{-0.7}$, where d_i is the electrode diameter in cm, ν is the kinematic viscosity in $cm^2\ s^{-1}$,

D_{lim} is the diffusion coefficient of the species that is under or near its limiting current density in $cm^2\ s^{-1}$and S is the electrode rotation rate in rpm. This Ni-Mo example is similar to the scenario in Fig. 5,*b*. A transport influence is expected in the Ni partial current density due to its low concentration in the electrolyte and high polarization of the electrode. If this was an uncoupled reaction, with an excess of molybdate in the electrolyte there should be no change of the Mo partial current density with the electrode rotation rate, but there indeed is. Thus, the Mo partial current density experiences a change in deposition rate due to the coupled nature of the Ni reduction reaction. The solid lines in Fig. 6,*a,b* are the modeling results of the equations given in Table 1, assuming that the side reaction and the Ni codeposition reactions have intermediates with very low surface coverage.

If tungsten reduction occurs primarily through a ternary, mixed-metal complex of some type, [Me-ligand-WO_4^{2-}], as presented by Younes and Gileadi [78], and Younes-Metzler *et al.* [70], Weston [18] and Belevskii [82], as opposed to an adsorbed intermediate, the apparent transport effect of the W PCD, when the concentration of the iron-group metal in the electrolyte is much less than the added tungstate species, $C_{Me(II)} << C_{W(VI)}$, would still manifest, as in Fig. 5,*b*. Hence, the W PCD would be limited by the available inducing ions to form the complex, and both metal PCD would mirror each other. This effect can be seen in the results of those reported by Younes and Gileadi [78] for the Ni-W codeposition system in citrate ammonia electrolytes. In the opposite scenario, if there was an excess of the inducing, iron-group element(s), $C_{Me(II)} >> C_{W(VI)}$, the formation of a ternary W complex would be limited by the amount of available W. Since the iron-group metal can be reduced independently, eqns (20) and (21), the PCD behavior would be represented by that in Fig. 5,*c*, giving an apparent decoupling of the W PCD with the iron-group element. To simulate essentially the same behavior as the Podlaha-Landolt model in Table 1, one needs to modify the governing equations in the bulk and at the electrode surface to account for the complexing equilibia.

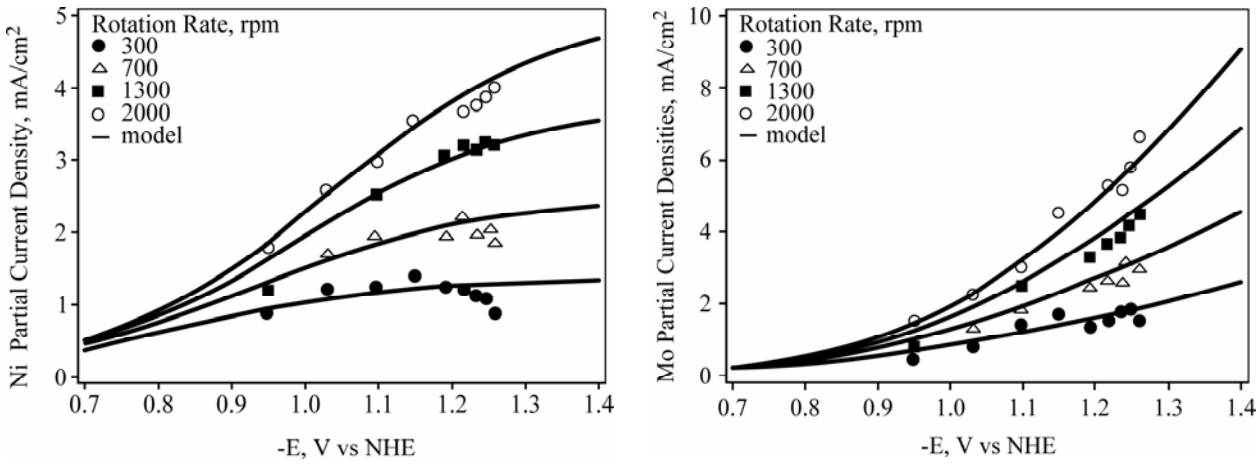

a *b*

Fig. 6. Partial current density of Ni and Mo, under the influence of a kinetic-transport control, showing an increase in the (a) Ni partial current density with electrode rotation rate and an induced rotation rate dependence, or apparent transport influence of the (b) Mo partial current density, when MoO_4^{2-} is in excess in the electrolyte; reproduced from ref [91], courtesy of the Electrochemical Society.

Differentiating between an adsorption model or a complexing species model for the induced codeposition of W (or Mo) is not straightforward with steady state polarization data. Electrochemical ac impedance spectroscopy does give an indication that adsorbed species are present, through the observation of an additional capacitive or inductive feature during Ni-Mo [92, 97], Ni-Fe [92], and Co-W [74] codeposition, which provides credibility to the adsorption model approach as adopted in the Podlaha-Landolt model. Impedance results of Chassaing *et al.* [87] were interpreted to be representative of a porous surface layer on Ni-Mo, which is more in line with a film model such as the one proposed by Vasko [10].

A limitation of the model in Table 1 is that it does not account for observable decreases of the PCD at very high overpotentials. Beltowaska-Lehman [98] observed that there is a decrease for both Ni and Mo PCD at applied potentials more negative than -1.3 V vs SCE. It is most pronounced with an increase in molybdate concentration, and attributed to the formation of molybdenum oxides. Analogously, Obradović *et al.* [99] observed a similar decrease in the total current density at high applied overpotentials in the Ni-W alloy system. In addition, the simulation of the PCD does not capture the region near the open-circuit potential and hence the thermodynamics of the system. Kröger [100] outlined changes in the activities described in the Nernst equation for systems that undergo abnormal deposition, including induced codeposition.

PROPERTIES OF TUNGSTEN ALLOYS WITH IRON GROUP METALS

Structure and thermal stability

The galvanic technique gives a wide opportunity to produce alloys of specific texture and nano- or amorphous internal ordering. Amorphous and nanocrystalline alloys have some specific mechanical properties. The grain size of electrodeposits depends on the electrodeposition technique used [101, 102], the chemical composition and pH of the electrolyte [47, 103] the current density [45], as well as on the substrate [104]. However, a specific internal structure of those types of hard and wear resistant materials is often combined with their severe brittleness.

The most critical factor determining the structure of electrodeposited tungsten alloys is the quantitative composition of the alloy. It was proved that by optimizing the DC plating conditions tungsten alloys with Ni, Co or Fe result in the formation of thermodynamically stable intermetalic compounds – Ni_4W, Co_3W and Fe_2W [48]. Those types of electrodeposited alloys are usually fully amorphous, hard and smooth films [47]. Investigations on the structure of electroplated Ni-W alloy performed by Donten *et. al* [46] indicated that this alloy has fibrous (columnar) structure and contains ultra-thin fibers (ca. 5 nm in diameter) oriented perpendicularly to the surface of the substrate. Single fibers aggregate and form broader columns when the thickness of the deposit extends to 1–2 micrometers. Such a phenomenon is well visible for Ni-W and Co-W alloys and less pronounced for Fe-W ones. This type of structure has implications on the physical properties of these materials. It was proved that the tungsten amorphous alloy exhibits strong magnetic anisotropy [105], breaks much easier in the direction normal to a substrate [106] and, because of its strong texture, probably has different hardness when measured in different directions.

When the alloys feature less amount of tungsten, they deposit in the form of a solid solution. In this case, tungsten is dissolved in the iron-group metal lattice. The material retains the structure of the base metal – Ni and Co are of the fcc type (Fm3m) and Fe has a bcc lattice (Im3m). The structures of deposits are often nanocrystalline with increased lattice parameters compared to pure iron group metals [86]. Usually, 16–18 at % of W in Ni or Co are the critical upper values for the formation of solid solutions. Changes in the alloys structure at these mentioned compositions, associated with the occurrence of a fully amorphous structure, have been reported in [107–108]. The deposits have also a strong (111) texture and exhibit an increase of (111) interplanar distance associated with an expansion of the lattice parameters, that is in the conformity with Vegard's law [47, 86]. In this case, increasing the tungsten content in the deposited alloy also decreases the crystal grain size, ranged from a sub-micrometers in materials containing several at. % of W to 5–10 nm, when the amount of tungsten exceeds 15 at. % [44].

Increasing the tungsten content beyond 18 at.% disturbs the solid solution structure of the electroplated tungsten alloys. Huang *et al.* [109] showed that a Ni-W electrodeposit with tungsten content at least of about 18 at% may consist of the Ni_4W intermetallic phase. Krolikowski *et. al.* [110] found out that the corrosion behavior of a nickel-tungsten alloy is significantly changing at ca. 18 at.% of W. At a higher tungsten content, the structure of intermetallic compounds probably becomes highly deformed. This phenomenon is described at large for Ni-W alloys. Sridhar *et. al* [111] also defined conditions for electroformation of Ni_4W. For the tungsten content from about 20 to ca. 35 at.%, electrodeposited alloys are fully amorphous [112–113]. Also Co-W and Fe-W alloys with a high tungsten content reveal amorphous (for Co-W) [68] or nanocrystalline structures, with the nanocrystal size smaller than 5 nm for Co-W [64] and for Fe-W [65, 114].

Tungsten alloys deposited in a pulse current mode also show an amorphous structure in the range of 18–35 at% of W; when compared to DC plated alloys, they turn to be more uniform and probably have a less pronounced columnar structure [58, 64]. Any further increase of the tungsten content in pulse electrodeposited alloys leads to the formation of other intermetallic compounds. Such deposits containing more than 35 at.% of W are described in a number of papers originating from Gileadi's research group. In general, while any chemical composition consisting of around 50 at% of W may contain a NiW phase, an increase of the tungsten content to about 66 at% leads to the NiW_2 phase. Younes *et al.* [71, 115] considered the formation of an orthorhombic NiW phase by XRD measurements, when the concentration of W in the deposit exceeded 40 at%. It was argued that formation of equal amounts of Ni and W in this case may be regarded as evidence, albeit circumstantial, for the existence of a tertiary nickel-tungstate-citrate complex. Later, Younes *et al.* also reported the first plating of a body-centered tetragonal NiW_2 phase [70]. As it was shown on XRD patterns presented in the aforementioned papers, alloys containing more than 40 at% of tungsten were not amorphous. It is worth noticing that alloys with the tungsten content exciding 40 at.% were obtained from the ammonia-free plating bath. The influence of ammonia and alkaline cations on the plating process and the structure of deposited alloys were considered by Zakharov *et al* [116].

It should be mentioned that the composition of tungsten-containing iron-group-metal alloys and their structure for some substrate materials can change with the thickness of the deposit (distance from the substrate) [46, 104, 117]. The similarity in crystallographic structure of the substrate and the selected components of the electroplated alloy (*e.g.* copper substrate and nickel from electrodeposited Ni-W alloy) can locally change the composition and structure of the deposits. However, these changes, visible on the cross-section of galvanic coverage, are limited to films not thicker than ca. 1 micrometer. Occurrence of this interaction between an electrodeposited layer and its substrate does not usually change the amorphous structure of the deposited layer but significantly improves its adhesion to the substrate [104].

Heat treatment can also change the structure and physical properties of tungsten alloys. Electrodeposited amorphous and nanocrystalline materials are usually thermodynamically unstable and tend to increase their grain size [48]; they often recrystallize when subjected to thermal treatment. The most severe changes in the internal structure are observed in amorphous alloys. Their metastable glass form is changed to a polycrystalline state of a lower potential energy [118]. Yamasaki *et. al*. [119] noticed a slow, systematic increase of size in nanocrystals of Ni_4W during annealing of $Ni_{75}W_{25}$ electrodeposited alloy. Up to temperature of 600°C, the increase of the crystal size was very slow. Longer heating of the material at 500–600°C resulted in the formation of ordered grains not larger than 12 nm in diameter. Above this temperature, the effect of recrystallization was significantly accelerated. After keeping the Ni-W alloy at 700 °C for 24 h, the mean crystal size increased to ca. 150 nm. Differential thermal analysis (DSC) indicated two exothermic phase transformations of nickel-tungsten alloy at temperatures of 610°C and 830°C. Those two signals were recognized as the formation of NiW and NiW_2 intermetallic compounds. This indicates that the amorphous structure of deposited alloys slowly transforms to nanocrystalline Ni_4W during annealing at moderate temperatures. In this process, the hardness of the coating significantly increases from a value of 770HV (as-deposited amorphous alloy) to 1450 HV (annealed nanocrystalline alloy with the grain size 12 nm).

Similar DSC experiments, supported by the observation of modifications in the magnetic properties of the electrodeposited $Ni_{80}W_{20}$ alloy, indicated phase transformation of the amorphous material appearing at a lower temperature range (400 to 500°C) [120]. In this case, two well-shaped DSC signals at temperatures of 431°C (0.34 J/mol) and 445°C (0.45 J/mol) were explained by the formation of the crystalline Ni_4W phase. Further increase of temperature, up to 800°C, indicated serious changes in the alloy structure and its magnetic susceptibility at temperature close to 650°C. Changes in hardness during the annealing process probably caused by structural modifications were observed during heat treatment of binary cobalt-tungsten and ternary cobalt-iron-tungsten alloys [121]. In this case, the highest hardness in alloys containing ca 25 at% of W was noticed after annealing at 600°C.

Exposing Ni-W and Co-W alloys to much higher temperatures leads not only to an increase of the crystal size of the solid solution and formation of intermetallic phases, but also to decomposition of the alloy with separation of carbides and metallic tungsten [114, 122]. As reported by Tsyntsaru *et. al*. [64], thermal stability of Co-W alloys depends on the content of tungsten in the deposit. While the deposits containing 24.5 at.% of W began the recrystallization process at 400°C, the alloys with higher ca. 35 at.% W retained their amorphous structure to almost up to 600°C. Similar transformation was also observed for electrodeposited Fe-W alloys. It was found out that recrystallization of alloys containing 23–30 at.% of W starts at temperatures above 400°C, but the nanocrystalline structure of the deposits does not change up to ca. 800°C. Elevation of the heating temperature up to 1000°C resulted in decomposition of the alloy to form Fe, Fe_2W and $FeWO_4$ crystalline phases [114]. The latter could be caused by recrystallization of oxides present on the surface and in cracks of the electrodeposits.

Results of investigations performed on ternary Ni-Fe-W and Fe-Co-W alloys indicated that significant, temperature-induced changes of those alloys occur at temperatures above 500°C and 700°C, respectively. The recrystallization of the amorphous/nanocrystalline Ni-Fe-W alloy [123] containing 10–14 at.% of W started at temperatures 500°C–600°C and led to the formation of γ-FeNi phase, Ni_4W and Fe_7W_6 intermetallic compounds. Because annealing of the alloys was performed in air, a large amount of material was oxidized to $NiWO_4$ and $FeWO_4$. Investigations on the thermal stability of Fe-Co-W alloy containing 50 at.% of Fe, 33 at.% of Co and 17 at% of W [124] revealed no changes in the structure at temperatures up to 600°C. Conversely, significant changes were observed for deposits annealed at temperatures above 800°C. In this case, the formation of nanocrystalline α-Fe phase was observed in XRD patterns and differential thermal analyses (DTA) plots. At the same temperature, the hardness of these alloys reached its maximum (ca. 1300 HV). Further increase of temperature resulted in fast recrystallization, with the formation of α-Fe, cubic Co and Fe_6W_6C phases.

Mechanical and tribological properties

Tungsten alloys with iron group metals possess attractive mechanical and tribological properties [18, 52–54, 56, 59, 63, 77, 106, 114, 121, 124–130]. A possibility of them to substitute conventional hard chrome plating from electrolytes containing Cr(VI) due to the toxicity of the hexavalent chromium species and volatility of them at high operating temperature of the chromium bath is often discussed in literature among a number of other applications of these alloys [18, 52, 53, 121, 131]. Industrial parts that are often hard chrome-plated include aircraft engines and landing gear, oil well equipment, crank shafts, hydraulic cylinders, paper making equipment, molds, stamps, dies, drill bits, and power industry equipment. The alternatives to hard chromium from aqueous-based electrolytes might be [131]:

– chromium coatings obtained from Cr(III) based solutions;
– nickel-base coatings (electroplated and electroless), alloys and composites;
– cobalt-base electroplates;
– plasma electrolytic oxidation.

In this section, hardness and wear resistance of electrodeposited tungsten alloys are mainly addressed to evaluate recent developments in investigation of nickel- and cobalt-base alloys with tungsten. Friction also is an important property, but considering and estimating the available data, it should be taken into account that it is partially a property of a sliding system that depends on a variety of interrelated mechanical, chemical, physical, and surface properties of sliding materials and surfaces [132]. Mechanical behavior depends on the deposit structure, composition as well as the electrodeposition operating conditions. The factors influencing the tribological and mechanical behavior can be broadly classified into internal and external factors.

Internal factors include recrystallisation temperature, crystal structure, grain boundary effects, etc., which significantly influence the shear strength of a material [134].

Recrystallisation temperature:

In some cases hardness is evaluated after heat treatment of coatings [124, 130], so direct comparison with data on as-deposited alloys is not straightforward [63, 114] because the structure changes after heating.

The highest hardness has been obtained for Fe-W alloys (1400 HV [114]), followed by heat-treated Fe-Co-W coatings (1140 HV [124]). In a descending order, we find Co-W alloys (800–1000 HV [18, 63]).

Nevertheless, this hardness is comparable to the hardness of the electroplated chromium under similar conditions of nanohardness measurement. Lower values were obtained for as-deposited Ni-W coatings [77, 129]. Ni-W alloy electrodeposition has been under investigation by many groups of researchers [52–54, 56, 99, 115, 128, 138–139]. However, some decrease in hardness after annealing was detected for Ni-Fe-W alloy [140]. Using metallic microstructures as mold inserts for hot embossing and injection molding requires hard and wear resistant materials in order to achieve an exact replication into polymers and ceramics [138]. The hardness and thermal stability of mold inserts were found to increase significantly with nickel-tungsten alloys. Nickel-tungsten alloys were employed for the manufacture of microstructured tools due to their excellent mechanical properties regarding wear and mechanical durability [138]. These tools have found applications in hot embossing and injection molding processes. As was previously noted [115], the concentration of W in the plated alloy has a major effect on its mechanical and chemical properties, such as hardness, abrasion resistance, and improved corrosion resistance at high temperatures. Then, the authors in [139] reported that the microhardness of Ni-W deposits was increased with an increase in the tungsten content in the alloy. Obradovic *et al.* [99] reported that Ni-W alloys exhibit such enhanced properties as corrosion- and wear-resistance, which makes them useful in practical applications.

Crystal structure:

Tribological behaviour depends on the crystal structure. For example, Wang *et al*. [135] compared nanocrystalline Ni and Co coatings upon fretting at equal grain sizes and microhardness and noticed that the wear rate of Co is much lower than that of Ni coatings. One of the possible reasons for this behavior stems from the difference in the crystalline lattice; namely, cobalt has hexagonal close-packed crystal lattice, which gives better tribological performance. Nevertheless, the performance of Ni coatings can be improved by alloying it with tungsten, as has been aforementioned [52, 54, 56].

Grain size and boundary:

The Hall-Petch relation, $H \sim d^{-1/2}$, correlates the hardness of a metal, H, with the inverse square root power on the mean grain size, d. However, the parameter d has been used interchangeably with the term "crystallite size" in the literature under review due to estimation of the particles sizes from XRD spectra. Still, as shown by Schuh [56], when particles sizes are relatively small (~ 10 nm), then crystallite and grain sizes obtained by means of the XRD and transmission electron microscopy (TEM) become close to each

other. Thus, in the present paper the term "grain size" will be kept, because the majority of the publications on tungsten alloys discussed (see Table 2) is in the "safe region" of less than 50 nm.

In the case of nanocrystalline alloys, at least two major factors contribute to hardening of those alloys: (1) formation of a solid solution (i.e., solid solution hardening), and (2) small average grain size [56], where hardening due to the formation of a solid solution in Ni-W alloy has weak effect compared to hardening observed in pure Ni was demonstrated, and a decrease in the grain size has a stronger effect. Similar investigations were made on Ni-W alloys by Yamasaki [54], for which the average grain size was even smaller (2.5–7 nm were attained when the tungsten content was the highest) than those in [56] (6–10 nm). It was observed that, when the grain size is decreasing from the micrometer range down to the nanometer range ~ 10–15 nm, the Hall-Petch relation is conserved, namely, with decreasing the grain size the hardness will increase [133]. When the grain size is below 10 nm, the Hall-Petch breakdown is observed, and a modulation and slight weakening of mechanical properties can be noticed [133]. Thus, Schuh in [56] stated that the Hall-Petch breakdown is observed for Ni-W coatings with grain sizes below ~ 8 nm. This value is lower than that of pure Ni (~ 14 nm), suggesting that alloying has suppressed the Hall-Petch breakdown Nevertheless, the mechanism of this breakdown is not well understood as some of the interrelated factors can affect the behavior of the coatings: structural changes, diffusion creep, the triple junction (at grain boundaries), increasing dislocations [134]. Thus, the mechanisms of deformation and the properties of the nanocrystalline materials depend on the average grain size, but are also influenced by the grain size distribution and the grain boundary structure (low / high-angle grain boundaries) [56, 134].

External factors like temperature, humidity, indentation size effect and contact conditions [132] are also attributed to effects, hence they should be taken into consideration when assessing tribological properties, *e.g.,* depending on the electrodeposition conditions impurities as carbon, sulfur or hydrogen can be incorporated into the coating [136] and have an impact on contact conditions during sliding and on hardness values as well. Additionally, copious hydrogen evolution from the side reaction during electrodeposition causes problems associated with micro- or nanovoids formation in the deposit, that sometimes yields contradictory results [133]. Besides, other parameters such as differences in the loads applied, initial roughness and different set-up for measuring mechanical and tribological properties can affect the measured values. Depending on the materials applied, hardness of the samples is a design-technological factor. The mutual arrangement of material hardness and counterbody may correspond to either a so-called direct friction pair (movable sample is harder than the fixed one) or a reverse friction pair (movable sample is softer than the fixed one). In higher kinematic friction pairs (line or point contact) the combination of materials "hard – hard" is also used.

Thus, the comparison of tribological and mechanical properties based on the published data is quite complicated because of different starting conditions of alloys deposition. A few studies can be compared to assess the wear rate of different tungsten alloys with the same set-up *e.g.* [63, 66, 114]. The Fe-W, Co-W and Co-W-P coatings were investigated in ball-on flat sliding tests against corundum ball counterbody. The Co-W coating possesses the lowest wear rate, even having the hardness a bit smaller (at 20 mN) than that of Fe-W or ternary alloys (Figs. 7–9). Noticeably, the grain sizes and tungsten content are very close to each other for the investigated alloys (see Table 2), suggesting that the alloying metal (Fe, Co) or grain boundary structure have an influence on the final hardness and tribological behavior. Weston *et al.* [18] also compared the tribological behavior of electrodeposited chromium coatings, nanostructured Co and Co-W electrodeposited alloys against steel counterbody. The wear rate of Co-W coatings was minimal in comparison to the electrodeposited pure cobalt and chromium coatings. Even at the maximum load, while the chromium coatings were worn out, Co-W underwent less damage. The results of that study are suggesting that Co-W alloys are best suited to replace chromium coatings.

The Fe-W alloy undergoes a severe tribo-oxidation during dry friction because iron oxidation causes an expansion of the wear track and cracks appear (see Fig. 7). Nevertheless, the tribological performance of Fe-W coatings can be highly improved under lubricated conditions [137] or by using ternary alloys such as Fe-Co-W [121, 124]. It should be mentioned that the authors in [124] did not compare binary Co-W or Fe-W coatings with ternary Fe-Co-W coatings under the same conditions; hence the comparison with other publications is a rough generalization.

Certainly all these factors, both internal and external, are interrelated in between them. The temperature of electrodeposition, pH, electrolyte composition and current (direct or pulse current or pulse reverse current [3, 10]) or potential applied do exert certain influence on the overpotential value and partial current of tungsten reduction and, eventually, on nucleation process of the given alloy, thus changing the crystal structure or preferential grow of crystals, grain size or grain boundaries. Thus, the growing interest in electrodeposited tungsten alloy coatings and structures, *e.g,* Co-W alloys [18, 59, 63, 77, 106, 121, 125, 127,

131] and Ni-W alloys [52–54, 56, 115, 99, 128, 138–139] will be further increasing because of the combination of mechanical, tribological and magnetic properties that these materials demonstrate in addition to corrosion resistance and catalytical properties.

Table 2. The relationship between structure and hardness for tungsten alloys

Conditions	Alloy	Concentration at. % W	"Grain size", nm	Hardness, HV	Load, g	Reference
Citrate-ammonia solution pH 9.2; 60°C	Co-W	2–15	–	450–680	10	[59]
Citrate -gluconate solution pH 6.0; 80°C.	Co-W Fe-Co-W	27	–	538–848	25	[121]
Citrate-borate solution pH 6.0; 40°C, pulse deposition	Co-W	0–7	6–50	800–1000	200	[125]
Citrate-ammonia solution pH 7.5	Co-W	10–17	14–19	620	5	[77]
Borate solution pH 3.5 – 6; 30 -60°C	Co-W	13	220–450	600	100	[126]
Citrate-borate solution pH 6.7; 60°C	Co-W	18–22	150–200	600–725	10	[127]
Citrate – ammonia solution pH 8.5, 75°C	Ni-W	8.4–12.7	20–22	500–570	100	[52]
Citrate-ammonia-borate solution pH 8.5; 75 – 85°C,	Ni-W	1–16	5–50	640	100	[53]
Citrate-borate solution pH 8, 80°C	Fe-Ni-W	7–28	200–300	550–630	300	[128]
Citrate-ammonia solution 72°C	Ni-W	11–13	4–10	611–815	1	[56]
Citrate-ammonia solution pH 7.5; 75°C	Ni-W	18–23	8–10	560–690	200	[54]
Citrate-gluconate solution pH 6; 80°C,	Co-W	14–25	5	500–1000	25	[18]
Citrate-ammonia solution pH 7-8, 70°C	Co-W and Fe-W	28	3–42	600–800	1–20	[106]
Citrate-borate solution pH 6.75; 58°C	Co-W	17–23	5–40	500–845	0.2–20	[63]
Citrate-ammonia solution pH 9.5, 65°C	Ni-W	15–30	–	650–800	15	[129]
Citrate-ammonia solution pH 8, 50°C	Ni-Fe-W	9–14	–	450–600	10	[130]
Citrate-ammonia solution pH 8; 70°C	Fe-W	23–30	3–5	700–1400	1–20	[114]
Citrate-ammonia solution pH 8; 80°C	Fe-Co-W	–	–	827–1141	98	[124]

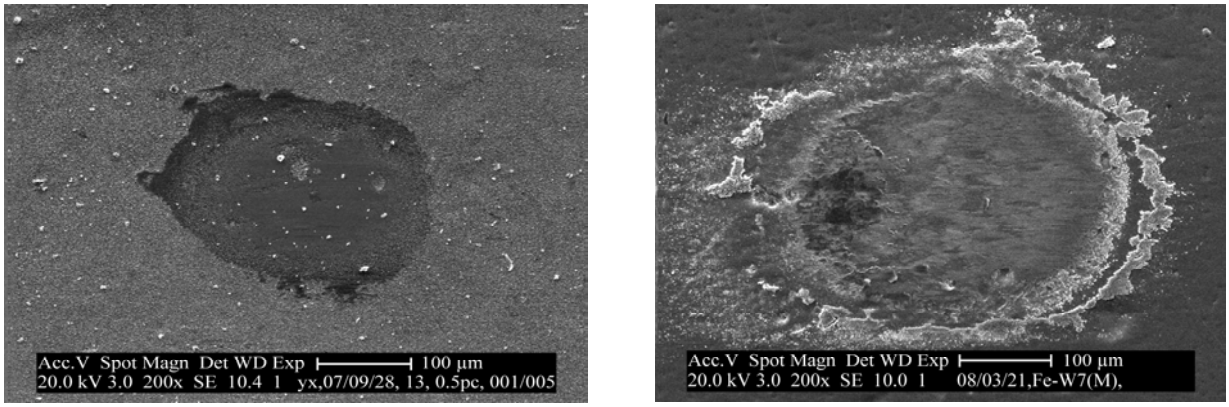

a *b*

Fig. 7. SEM images of coatings after dry sliding under normal load of 2 N: (a) Co–W and (b) Fe–W alloys.

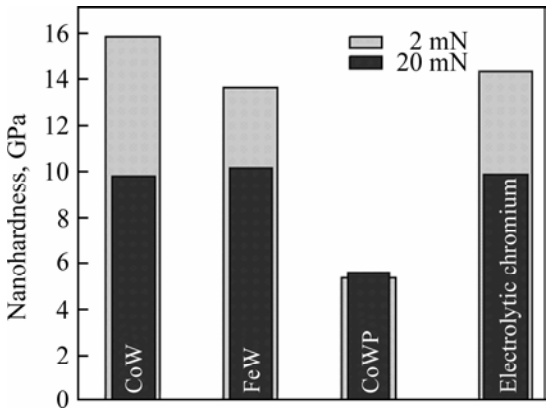

Fig. 8. Average nanohardness of tungsten alloys in comparison with electrolytic chromium and Co-W-P. Graphs are prepared based on the data published in [66].

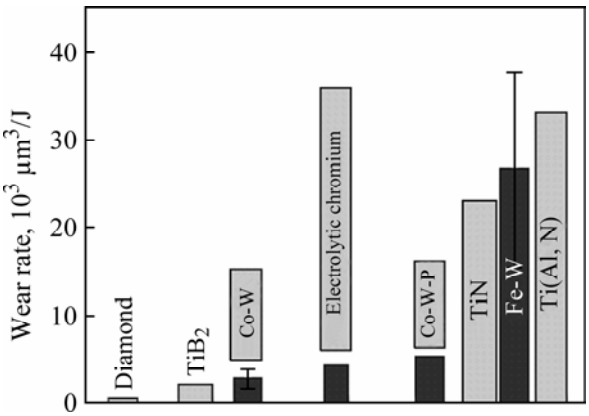

Fig. 9. Wear rate of tungsten alloys in comparison with other hard coatings. Graphs are prepared based on the data published in [66].

Corrosion properties

Today materials for applications are frequently selected according to their functional properties. The electrodeposition of films and electroforming are promising methods to be applied in galvanotechnics. Due to a large surface–area-to-volume ratio of thin films, as compared to that of bulk materials, the properties of thin films, as a rule, significantly differ from the bulk (macro-scaled) materials behavior. Film composition, microstructure and density are very much dependent on preparation methods and conditions. The variation in corrosion rates and other properties of the surfaces with the fabrication method and structure are well known [141, 142]. Then, differences in corrosion properties between cast iron-group metals and the corresponding electrodeposited metals have been observed. The values of corrosion potential (open circuit potential – OCP) are more negative for the electrodeposited metals than for the corresponding cast metals. Furthermore, higher corrosion currents are obtained in electrodeposited metals [143]. Therefore, the examination of the corrosion properties of the obtained materials is an integral part of the modern materials science and crucial in terms of technological applications. In the meantime, the unique combination of tribological, magnetic, electrical and electroerosion properties of tugsten alloys has triggered an increased potential of these materials in macro-, micro-, and nanotechnics. Indeed, a fundamental requirement for materials in microtechnology is that they show an extremely high corrosion resistance. This is due to the continuous decrease in the component size, down to the micrometer range. Under such conditions, the resistance to device failure due to even a small amount of ionic contaminants may become a key issue in terms of lifetime and reliability.

Tungsten (as well as molybdenum) alloys show a relatively low hydrogen overvoltage [144], and corrosion of tungsten (and molybdenum) alloys with iron group metals undergoes mainly with hydrogen depolarization. Moreover, the absolute values of both hydrogen evolution reaction and anodic reaction have to occur at the same rate, while leaving the alloy in the corrosive media. These are important factors governing the relatively negative values of corrosion potential and the rate of corrosion, which in some cases (*e.g.* Co-W) correlates well with exchange current density for hydrogen evolution [145].

Tungsten alloys with iron group metals hardly transfer into a passive state in neutral solutions [110, 146, 147]. The shapes of Evans diagrams of all investigated freshly electrodeposited alloys reveal a non-passive state [66, 148]. Even after exposing these materials for 15 days in open air, the corrosion potential shifts towards more positive potentials by 100–200 mV, but remains relatively negative. Therefore, the rubbing of surfaces does not promote corrosion, i.e. tribocorrosion of such alloys might be relatively weak. When tungsten alloys are exposed in open air for 6 months, the corrosion potentials shifts towards positive values by 0.4-0.5 V compared with values of corrosion potential of freshly electrodeposited alloys. The tribocorrosion testing was carried out on electrodeposited nanocrystalline Fe-W (26 at.% W), Co-W (28 at.% W); Co-P-W (4,5 at.% P, 20 at.% W) alloys exposed to ambient air for 6 months. Based on corrosion potential measurements and electrochemical impedance data, the corrosion resistance under sliding conditions in 1M Na_2SO_4 at 5 N load decreases in the sequence: Fe-W>Co-W>Co-P-W [146].

The corrosion behavior of nanocrystalline ("amorphous-like") tungsten alloys is intriguing, as one can expect that the increase of the amount of tungsten in the coating will increase its corrosion resistance. Ni-W alloys electrodeposited from a citrate solution consist of three different phases, which are all present in high W-content alloys: a solid solution of W in a Ni matrix; an intermetallic compound Ni_4W, as well as another solid solution of W in Ni, with a W content higher than 20 mol. %. The XPS analysis revealed that the alloys were covered with a surface layer of a complex structure containing pure metals Ni and W, $Ni(OH)_2$ and WO_3, on the very surface, as well as some partially reduced oxide $WO_{2.72}$ (most probably a

solid solution of $WO_{2.72}$ in Ni) and tungsten carbide in the layer underneath. It is highly probable that some of the oxide species in the layer act as intermediates in the cathodic deposition process. Identifying these species should be the clue to a more detailed understanding of the mechanism of induced deposition of W than has been achieved so far. Corrosion of Ni-W alloys in sulfuric acid solution at corrosion potential occurs by the preferential dissolution of nickel from the surface layer. The longer the corrosion process lasts, the more the surface behaves like pure W. The lowest initial corrosion rates were recorded with alloys rich in W, but after aging at OCP the lowest corrosion c.d. was found for the Ni-W alloy with the most homogenous phase structure, consisting of the solid solution only [149]. Based on the data obtained in neutral and acidic sulphate solutions presented in [66, 110, 143, 148], it can be stated that resistance to corrosion of nanocrystalline tungsten-rich alloys decreases (i.e. corrosion currents increases) in the following order: Ni-W; Co-W; Fe-W. However, there are still some ongoing controversial issues that deserve further investigation. Namely, while the experimental data presented in [145, 150] showed that the best corrosion resistance was achieved in the cases of Co-W and Ni-W coatings with a lower content of tungsten, other authors [110] demonstrated that all tested Ni–W coatings containing 11–21 at.% W exhibited a quite comparable corrosion resistance in NaCl solution. Probably, the rate of corrosion of tungsten alloys depends on both composition and structure of the deposited alloy. Amorphous alloys, whatever way they are prepared, are metastable. In turn, nanocrystalline materials have a large fraction of mass concentrated at grain boundaries; therefore they are also in a metastable state due to an excess of free energy stored at these grain boundaries that can be reduced in the course of a higher local corrosion rate. On the other hand, the alloys having larger grains corrode at lower rates. Consequently, on progressive heating, an amorphous/nanocrystalline alloy will first lower its energy by relaxation to a more stable state and at a higher temperature it will tend to crystallize, thus resulting in an increase of the grain size. Therefore, the rate of corrosion after annealing amorphous-like alloys decreases, e.g Fe- W [151], Fe-Ni-W (with 55 wt.% of W) [128]. It is also worth mentioning that the corrosion resistance of amorphous-like tungsten alloys with iron group metals can be improved by introducing phosphorous as an alloying element. The corrosion potential is moved towards more noble values by adding P to the deposit, and the passive current density then drops remarkably with the addition of W. Hence, amorphous Ni-W, Ni-W-P, and Fe-W alloy deposits show very high corrosion resistance in acid solutions [152].

Magnetic properties

Because of the outstanding mechanical, magnetic and corrosion-resistance properties, electrodeposited tungsten-containing alloys have been proposed in recent years for a widespread variety of magnetic applications, ranging from recording media [29, 105] to remotely-actuated micro-/nano-electromechanical systems (MEMS/NEMS), such as microactuators, micromotors, sensors, microgears or micromechanical magnetometers [153–155]. Amongst the investigated films are: binary alloys (*e.g.*, Co-W [153–159], Ni-W [29, 105, 160], Fe-W [160]), ternary alloys (*e.g.*, Co-Pt-W [161] or Ni-Fe-W [162]) or even more complex systems (*e.g.*, Co-Pt-W-P [161, 163] or Co-Ni-Re-W-P [164]). Magnetic properties of these alloys (coercivity, H_C, anisotropy easy axis direction, saturation magnetization, M_S, squareness ratio or remanent-to-saturation magnetization ratio, M_R/M_S, etc.) depend not only on the composition but also on the microstructure of the obtained films.

Both hard and soft ferromagnetic properties have been reported in electrodeposited Co-W alloys (see Table 3), depending on the exact electrodeposition conditions (in particular, the applied current density, *j*). In many Co-based alloys (including Co-W), the microstructure of films consists of isolated ferromagnetic Co-rich grains surrounded by non-magnetic or weakly-magnetic boundaries, where alloying elements (*e.g,* W, P, Pt, Mn) tend to concentrate [153]. However, Co-W films with a more uniform microstructure have been also prepared by electrodeposition using aqueous baths as electrolytes, with and without organic additives [154, 156–159]. Alloys with tungsten weight percentages of up to 30–40% have been readily obtained [155, 159]. Remarkably, while the alloy composition does not depend significantly on the applied current density (*j*), the microstructure of films becomes progressively more refined as *j* increases, leading to pronounced variations in the coercivity and squareness ratio values. The formation of hard-magnetic hcp Co_3W is usually promoted when films are prepared at low current densities [157], whereas larger *j* values render amorphous Co-W films with concomitantly lower coercivity, both along in-plane and perpendicular-to-plane applied field directions. The coercivity of Co_3W films also markedly depends on the degree of texture [157]. Typically, a (001) texture develops during growth of Co_3W hcp films, favoring the occurrence of hard ferromagnetic behavior and perpendicular-to-plane magnetic anisotropy [155]. Conversely, fcc and amorphous Co-W are magnetically softer [154, 157, 158]. It is also possible to prepare Co_3W/Co-W multilayers, where H_C and M_R/M_S can be precisely tuned by varying the layers thickness [154, 158]. The exchange coupling between both phases causes the formation of kinked hysteresis loops, typical of spring-magnet be-

havior [165]. As expected, the saturation magnetization of Co-W alloys tends to decrease with the W percentage [157]. However, a further reduction in M_S is observed when films become amorphous [158].

Table 3. Summary of magnetic properties* of different W-containing alloys

Composition	Microstructure	M_S (Tesla)	M_R/M_S	H_C (Oe)	Reference
Co-W (6–44wt% W)	Amorphous for high current density	1–1.5	0.2–0.8 (∥)	20 (∥) 30 (⊥)	[154, 157, 158]
Co_3W	(001) hcp textured films (<*D*> = 10–60 nm), low/intermediate current density	~1.4	0.2–0.5 (∥) 0.3–0.7 (⊥)	200–600 (∥) 50–900 (⊥)	[156-159]
Co_3W/Co-W	hcp Co_3W + fcc/amorphous CoW (spring-magnet); multilayers	1.2–1.3	0.2–0.5 (∥)	3–250 (∥)	[154, 158]
Ni-W	Nanocomposite films	0.3–0.6	~0.05 (∥)	~10 (∥)	[160]
Fe-W	Nanocomposite films	~1.8	~0.05 (∥)	~10 (∥)	[160]
Ni-W	Columnar fcc grains	0.4–0.6	0.1–0.6 (∥) 0.1–0.8 (⊥)	160–650 (∥) 250–1500 (⊥)	[29, 105]
Ni-Fe-W	Nanocrystalline fcc grains ((<*D*> = 25–40 nm)	0.6–1	~0.05 (∥)	~10 (∥)	[162]
Co-Pt-W-(P)	Columnar hcp grains; ⊥ anisotropy favored by the (001) texture	0.8–1	0.05– 0.5 (∥) 0.1–0.7 (⊥)	60–2450 (∥) 650–2720 (⊥)	[161, 163]
Co-Ni-Re-W-P	Columnar hcp grains with (002) texture	~1.2	0.05–0.1 (∥) 0.15–0.3 (⊥)	~100 (∥) 500–2500 (⊥)	[164]

*) H_C, M_R and M_S denote the coercivity, remanent magnetization and saturation magnetization, respectively. The symbols ∥ and ⊥ indicate results from hysteresis loops recorded along the in-plane and perpendicular-to-plane directions, respectively. <*D*> refers to the average crystallite size, as evaluated from x-ray diffraction experiments.

In addition to Co-W, other binary W-containing electrodeposited alloys (*e.g.*, Ni-W or Fe-W) have been also electrodeposited. These films can exhibit either hard [29, 105] or soft [160] ferromagnetic properties, depending on the microstructure. Soft ferromagnetic properties (i.e., low H_C and M_R/M_S ratios) have been reported in composite coatings consisting of W particles embedded in Ni or Fe films [160]. Hard ferromagnetic behavior, with perpendicular-to-plane coercivity values ranging between 250 and 1500 Oe, has been obtained in Ni-W films (W weight percentage in the range 6 –18%) consisting of columnar Ni-W fcc grains of about 5–25 nm in lateral size, with (111) texture, embedded in a Ni-W amorphous matrix. Similar to Co-W alloys, the saturation magnetization of Ni-W films decreases with the W content, not only because of the inclusion of non-magnetic W atoms (dilution law) but also due to the pronounced reduction in the crystallite size that occurs for high W percentages [29, 105].

Enhanced hard magnetic properties (*i.e.*, permanent magnet-"like" behavior) have been reported in Co-Pt-W-(P) electrodeposited alloys, with coercivity values as high as 2450 Oe and 2720 Oe along the in-plane and perpendicular-to-plane directions, respectively [161, 163]. Again, texture effects seem to play an important role in the observed anisotropy direction. While (001) crystal orientation favors perpendicular-to-plane magnetic anisotropy, the occurrence of other preferred orientations promotes in-plane anisotropy easy axis. Interestingly, post-synthesis chemical treatments of Co-Pt-W-(P) films in H_2SO_4 solution have been found to be beneficial for the increase of the H_C and M_R/M_S values of this type of films, although a two-fold decrease in the saturation magnetization is observed [164]. Contrary to Co-Pt-W-(P), Ni-Fe-W alloys exhibit soft ferromagnetic behavior, with the coercivity lower than 10 Oe and the saturation magnetization up to 1 T [162].

Finally, hard ferromagnetic behavior has been also encountered in Co-rich electrodeposited Co-Ni-Re-W-P alloys, with Co and W weight percentages around 70% and 7%, respectively [164]. The coercivity value in these films, measured along the perpendicular-to-plane direction, ranges between 500 and 2500 Oe and the M_R/M_S ratio between 0.15 and 0.3, whereas hard-axis loops with low coercivity are measured along the in-plane direction (Table 3). The perpendicular magnetic anisotropy can be ascribed to the prominent (002) hcp crystallographic texture. Remarkably, due to the shape anisotropy, the squareness ratio of this material can be further increased, up to $M_R/M_S = 0.45$, if the continuous films are patterned to form arrays of

micro-cylinders with a 2:1 length:diameter aspect ratio [164]. Aside from the obvious use of these hard-magnetic alloys in high-density recording media, other applications can be also envisaged, such as microactuators and magnetic sensors [164].

APPLICATIONS OF TUNGSTEN ALLOYS

Hydrogen electrocatalysis

One of the most attractive applications of W alloys is the electrocatalytic production of hydrogen. Hydrogen is considered to be the energy vector for the future and its production, storage, and transportation are currently receiving a great deal of attention. This has prompted a lively research of new materials able to fulfill the demands of the sustainability in the energetic sector. In this context, Ni-W alloys have been proposed as electrocatalysts for hydrogen production since they offer lower overpotentials for the hydrogen evolution reaction (HER) than pure Ni. This has, in turn, stimulated the research on the electrodeposition of Ni-W alloys and the assessment of their HER properties. In principle, crystalline materials are preferred over amorphous ones because the former are more active for the HER due to a larger number of electrochemically active sites on crystalline surfaces. In any case, studies in this field are still not numerous and it is envisaged that the interest on the electrodeposition of W alloys will experience a revival in the near future. The HER on electrodeposited Ni-W alloys has been studied both in alkaline and acidic media [28, 166–170], and even when the Ni-W is deposited *in situ* with the catalyzed hydrogen [169]. Navarro-Flores *et al.* [28] considered crystalline $Ni_{3.4}W$ with a high intrinsic electrocatalytic activity, explained that by the modification of the electron density in *d*-orbitals upon alloying nickel with tungsten. It also have been observed that an increase in crystallinity leads to an enhancement of the HER. In constrast, according to Wang *et al.* [170] amorphous alloys electrodeposited under a super gravity field exhibit enhanced HER activity in 10% NaOH solution compared to the activity of those deposited under normal gravity conditions. Those authors showed that the quality of Ni-W layers had important implications on the HER properties. While the layers deposited under normal gravity conditions consisted of nodular grains and featured microcracks, those deposited under super gravity fields were fine-grained and crack-free. As a result, the current density of the HER at an overpotential of -150 mV vs. SHE increased from 3.3 mA cm^{-2} to 82 mA cm^{-2}. Such an increase was attributed to both the increase in surface roughness and the intrinsic activity.

Moreover, Navarro-Flores *et al.* [28] studied the HER in 0.5 M H_2SO_4 solution at 22ºC by the Tafel linear polarization measurements for pure Ni and $Ni_{3.4}W$ (23 at% W) electrodeposits. They found out that the pure Ni coating exhibited the classical Tafelian behavior within the explored overpotential window (between -0.5 and 0 V vs. SHE), indicating that the HER was a kinetically controlled Volmer-type reaction. Conversely, the HER kinetics for the $Ni_{3.4}W$ coating was controlled by the Heyrovsky desorption at low overpotentials and by the Volmer reaction at higher overpotentials. The Tafel value thus increased from 40 mV dec^{-1} to 123 mV dec^{-1}. Such a change in the Tafel slope was mainly attributed to the increased ability of $Ni_{3.4}W$ to form hydrides compared to pure Ni, as demonstrated by electrochemical impedance spectroscopy (EIS) experiments. The authors in [28] estimated that the amount of energy (*i.e.,* the overpotential) required to maintain a fixed current density of 1 mA cm^{-2} and thus a fixed hydrogen production rate was -379 mV for Ni and -85 mV for $Ni_{3.4}W$ (i.e., 80% lower power input). Indeed, the $Ni_{3.4}W$ electrodeposit displayed a higher intrinsic electrocatalytic activity, likely due to an increased electron density around Ni-sites.

The electrocatalytic performance toward the HER of a series of Ni-based alloys prepared by electroless deposition was studied [171]. Ni-W-P and Ni-Mo-P alloy electrodes exhibit good electrocatalytic activity toward HERs, with some Ni-Mo-P alloys approaching the performance of Pt foils. The electrocatalytic activity of Ni-based alloys decreases with increasing P content but increases with increasing content of W or Mo. The experimental results can be interpreted in terms of a pronounced synergy between Ni, which has internally paired *d*-electrons, and W or Mo, which have empty or half-filled *d*-orbitals and therefore, bind hydrogen atoms strongly. The absorption of hydrogen in these alloys is also found to have an important effect on their activity. Electrodes with higher activity are capable to incorporate larger amounts of hydrogen during cathodic charging.

It has been recently demonstrated that the HER activity of Ni-W electrodeposits can be enhanced if the two metals are codeposited with suitable metal oxide particles. In [172], Ni-W/TiO_x composites were potentiostatically deposited onto pristine carbon fibers and the HER was studied in 0.5 M H_2SO_4 at -500 mV vs. SCE by the EIS. The Ni-W/TiO_x-coated carbon fibers showed lower charge transfer resistance (i.e., a higher HER activity) compared to that of the Ni-W-coated fibers.

The usefulness of Ni-W electrodeposits as a cathode in microbial electrolysis cells (MECs) has been also investigated by Hu *et al*. in [173]. They demonstrated the hydrogen production in a single-chamber tu-

bular MEC equipped with a Ni-W alloy electrodeposited onto carbon-fiber-weaved cloth that served as the cathode. At an applied voltage of 0.6 V the MEC exhibited a hydrogen production rate of 1.5 m^3/day/m^3. Though the hydrogen production was lower when compared to the Pt cathode (2.3 m^3/day/m^3), this study demonstrated a great potential of Ni-W alloys as cathode materials in MECs. Also, the replacement of platinum metals in catalysts by Ni-W alloys is discussed based on the exchange currents of hydrogen evolution reaction [174]. The results of this study allow concluding that nickel-tungsten alloys containing 15–35% deposited on nickel are the most perspective catalytic materials of non-platinum group.

Compared to Ni-W, the HER in the electrodeposited Co-W alloy films has been scarcely reported [175–177]. The exchange current density (ECD) of hydrogen evolution as a function of the content of Co-W alloys was reported in [145]. It was determined that for hydrogen evolution as a function of the content of Co-W alloys has a minimum corresponding to transitive from polycrystalline to nanocrystalline structure (20–22 at.% of W); the values of the Tafel coefficient for Co-W alloys are in the range 90–130 mV dec^{-1}. Aravinda *et al*. [81] showed that the HER in alkaline citrate-containing solutions (pH 8.0) was enhanced by an increase in the concentration of either tungstate ions or dimethyl sulfoxide (DMSO) during the deposition of a Co_3W film. According to the authors, the adsorption of DMSO molecules onto the electrode surface would favor the electrochemical discharge of water since these contain sulfur, which is as a well-known reducing agent.

Deposition into recesses

Microstructures

Novel microdevices can be realized by merging electrodeposition with substrated, pattered with UV, lithography, high energy X-ray or e-beam lithography. The fabrication of new MEMS, made up of mechanical, fluidic, and electrical elements of micrometer scale, has the potential to change our way of life in future as dramatically as microelectronics has transformed it today. Its range of dimensions gives a possibility of mixing nano-, micro- and macro-structures fabricated with extreme precision with the same processes. The versatility of high aspect ratio microfabrication processes permits the manufacture of truly three-dimensional microstructures. In order to realize these structures deep imprints are made into a polymeric resist and are filled with metals using electrodeposition. Precisely machined high aspect ratio structures are thus possible. The choice of electrodeposition as a method for depositing metals into microstructures is motivated by the low capital investment requirements, and elimination of subtractive patterning procedures. The resulting metallic structure is used either as the final product or as a mold for plastic processing.

Single metals or alloys can be electrodeposited into deep recesses for MEMS production. Alloy deposition is inherently more difficult to control than single metal deposition but it offers a wider array of tailored material properties. A review of a variety of metal alloys deposited into MEMS structures is given by Ehrfeld, *et al.* [26], including their proprietary structures with Ni-W.

Recently, an increasing interest in electrochemical alloy deposition has emerged as a result of novel microfabrication techniques for micromachines by the LIGA process [178–180], (LIGA is a German acronym that stands for: **Li**thography, **G**alvanoformung – *Electrodeposition,* **A**bformung – *Plastic Molding*), and generally refers to the use of high energy x-rays, produced at a synchrotron, in resist exposure for the lithographic step. The LIGA process was one of the first high aspect ratio microfabrication processes, which was principally developed at the Institute for Microstructure Technology at the Nuclear Research Center, Karlsruhe, Germany (IMT-FzK) in response to the need for precisely machined nozzles having high aspect ratios, principal dimensions of tens of micrometers, and precise vertical sidewalls [178, 179]. Subsequent research at the IMT-FzK, the University of Wisconsin and other laboratories has further refined the process and produced numerous device prototypes, *e.g.,* see [181, 182]. Sharp corners and vertical sidewalls are obtained; deviations from the vertical of only 0.055 μm/100 μm over a height of 400 μm have been verified [183]. Resist layers up to ten centimeters thick have been patterned, making the fabrication of structures with aspect ratios much greater than 100:1 possible. The exposed and developed resist can be subsequently used as a substrate for an electroplating process. The metal structure can also be used as a mold insert, for plastic molding, to fabricate large volumes of plastic micro-scale parts. Tungsten alloys may be a choice material to fill this niche in developing micromolds and multiscale molds.

Reports of tungsten alloy plating in LIGA microstructures have generally centered on electrodeposition of tungsten alloys using known electrolytes and measuring the resulting properties; rightfully so, as the property is the key parameter in adopting tungsten alloys. As an alternative to LIGA Ni, particularly for high-temperature MEMS applications, the tungsten alloy can greatly improve microstructural instabilities and loss of mechanical strength at intermediate temperatures when compared to Ni microstructures [183–188]. Replacing electrodeposited Ni with an electrodeposited Ni-W alloy has improved MEMS struc-

tures at elevated and cycled temperatures as noted and reviewed by Suresh *et al.* [189] and Haj-Taieb *et al.* [190], but with lower ductility, fracture toughness and increased internal stress than Ni. In both reports [189, 190] electrodeposited Ni-W microtensile specimens with a thickness of 150 μm prepared using the LIGA process, and deposited from an ammonium citrate bath. Suresh *et al.* [189] showed a Hall–Petch plot of the measured yield strength of Ni–W samples as a function of the inverse square root of grain size with a marked increase in yield strength with the addition of 5 and 15 at % W and found out that the underlying microstructures of the Ni–W alloys are stable up to 700^0C. Those researchers concluded that as-deposited Ni-W exhibits brittle failure, but annealed LIGA Ni-W samples had a superior mix of thermal stability, strength and ductility. Haj-Taieb *et al.* [190] investigated various annealing temperatures. They observed a small grain growth, compared to electrodeposited LIGA Ni deposits, with micro-hardness values of the LIGA Ni-W higher than those of the pure LIGA nickel. The 15 at % W structures exhibited a smaller decrease of the hardness with an increase of the annealing duration. Tensile tests reported the ultimate tensile strength (UTS) above 750 MPa, but lower ductility than pure nickel. Armstrong *et al*. [191] were the first to design a methodology to measure fracture toughness of micro-scale specimens. They electrodeposited Ni-W alloys from an ammonia-citrate electrolyte [52, 108] with beam structures having nominal dimensions of 60 μm×20 μm×14 μm. The load applied using a nanoindenter and fracture toughness, calculated from the fracture load was in the range of 1.49–5.14 MPa√m for a Ni-W structure containing 12.7 at.% W. This is a higher fracture toughness of Si (another important MEMS material), but unfortunately considerably lower than that of electrodeposited nickel and other nickel-based alloys.

Electrodeposited Ni-W into recesses can be problematic if there is high internal stress, and microstructures that can potentially be tens to hundreds of microns tall could develop cracks. Several investigators made reports on using sulphamate nickel salts in ammonium-citrate electrolytes: Wang *et al*., [192] and Namburi and Podlaha *et al.* [193], and from boric acid-citrate, non-ammonia electrolyes, Slavecheva *et al.* [27], for the purpose of reducing internal stress. It is interesting to note that the authors of these two papers have observed a significant decrease of W % in the deposit compared to thin films. This can indicate the problematic nature of species under diffusion control with an enhanced boundary layer due to the depth of the recess. In particular, even if the reacting metal ion species are not under diffusion control, the resulting hydroxyl ion produced by the deposition reaction can be. In this case, the local pH can increase and alter the deposit composition.

An example of a tall, 500 μm Ni-W deposit from an ammonia-citrate electrolyte is shown in Fig. 10. The electrolyte contained 0.25 M sodium citrate, 0.4 M sodium tungstate, 0.2 M nickel sulfate and sufficient ammonium hydroxide to obtain a pH of 10. The deposit was pulse plated between -17.5 mA/cm^2 and current density with long pulse times, with on-time = 15 s and off-time = 45 s. With this particular choice of electrolyte and current density, dc deposition at the same current density did not result in a deposit, but a clear precipitation of salts was visually observed, indicative of a large surface pH rise. Key to the design of the pulse plating conditions is that sufficient time is chosen to match the diffusion time scales of the hydroxyl ion from the bottom of the recess. Hence, the pulse off-time is on the order of many seconds as opposed to fractions of a second for conventional pulse plating. The composition was measured at 20 equidistant points along the length of a micropost, with the wave-length dispersive x-ray analysis (WDS), and the composition was found to be uniform but low, having 3 wt % W along the direction of growth.

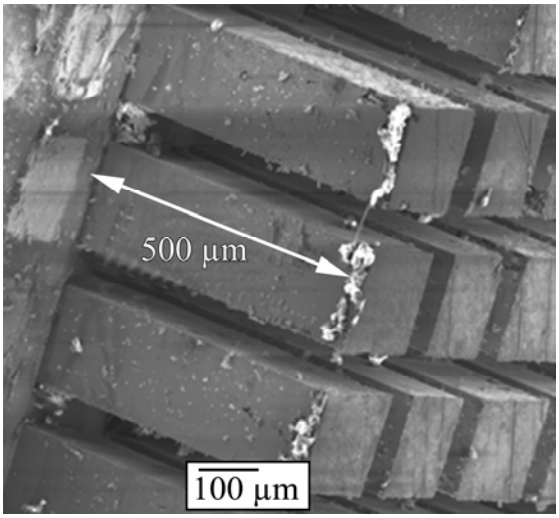

Fig. 10. Example of a tall, 500 micron Ni-W structure with 3 wt % W [193].

Nanowires of electrodeposited alloys can be readily fabricated through templating techniques into nanoporous membranes,which has been widely demonstrated, mostly in the area of magnetics [194–196]. A particular niche of the electrodeposition process is that it is the preferred, and in some cases the only, process that renders the deposition of multilayered nanowires, which has been used to deposit giant magnetoresistant materials (GMR), where a change in the magnetic field changes the deposit resistance. Nanowires with nanolayers of a ferromagnetic magnetic material separated by a non-ferromagnetic material, such as Cu, can easily present the current-perpendicular to the multilayer plane (CPP) type of GMR as opposed to the current-in-plane (CIP) GMR for thin films, providing more sensitivity [197–199]. There are numerous electrodeposition examples of nanowire, multilayered alloys in literature,, such as systems with Co-Cu/Cu [200–205], Co-Ni-Cu/Cu [206–208], as well as electrodeposited alloys nanowire arrays that are unlayered for non-GMR magnetic applications, for example, Co-Ag [209,210], Ni-Fe [211] Ni-Co [212], Ni-Cu [213] and Ni-Fe-Co-Cu [214].

In a study to develop a Cu-Ni-W nanowire alloy with the ability for composition modulation, Gupta and Podlaha [215] used an ammonia-citrate electrolyte with 60 μm thick, commercially available anodized aluminum oxide membranes (Whatman, Anodisc 25), with a listed pore diameter of 20 nm. Multilayered alloys with one layer rich in Cu and the other layer rich in Ni-W were fabricated. The electrolyte contained 0.6 M $Na_3C_6H_5O_7$, 0.2 M Na_2WO_4, 0.3 M $NiSO_4$ and variable $CuSO_4$ concentrations at the pH = 8, adjusted with ammonium hydroxide at 70 ± 2°C. Since copper is more noble than nickel or tungsten, it can be preferentially deposited at a low current density; and an alloy rich in Ni-W with some Cu can be deposited at a high current density. Due the presence of ammonia in the baths, the reversible potential of copper is shifted to a more negative potential range, hindering the ability to form multilayers with a pure Cu layer. Without ammonia, there is a larger separation of the reversible potential of copper and nickel-tungsten, that facilitates multilayer fabrication, however a lower ammonia concentration or no ammonia lowers the current efficiency appreciably for nickel-tungsten codeposition without addition of an alternative buffer, such as boric acid. Moreover, the nanowire deposition was confounded by the formation of oxide during the modulation, and results therein recommended that the potential of a more noble step be more negative than -0.9 V vs SCE to avoid this situation.

Bairachna, *et al.* [216] electrodeposited Ni-W alloys from a non-ammonical electrolyte, containing citrate and boric acid. Deposition was carried out in polycarbonate membranes that are much thinner, hence provoking less of a change in transport boundary conditions when compared to thin films than the alumina used in the previously cited study. Nanowires were successfully deposited with dc or pulsed current density. A typical example of released nanowires using dichloromethane to dissolve the membrane is shown in Fig. 10, with two types of measurements. The diameters of the nanowires are between 135–155 nm due to nondiscrete edges. The surface of the nanowires appears to be modulated, that is irrespective of whether the deposits are dc or pulse plated, and some of the measurements in Fig. 11 show the size of bumps (~30–40 nm). The modulation effect may be similar to the laminations first noted in thin films by Brenner *et al*. [6] in 1947, that also occurred when the current was not pulsed or interrupted.

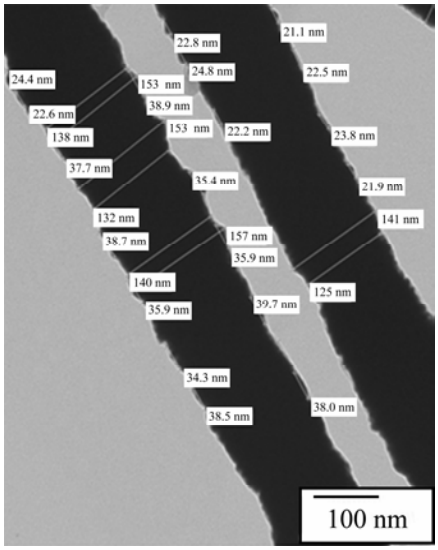

Fig. 11. TEM of pulsed current Ni-W deposit from Whatman polycarbonate membranes with a stated pore diameters of 50 nm at one end; actual pore diameter varies slighlty along length, ω (W) = 50.4 ± 0.5 wt.%. (with permission from the Electrochemical Society) [206].

Cesiulis *et al.* [67] developed conditions to electrodeposit Co-W-P and Co-W into nanoporous alumina oxide membranes, utilizing an electrolyte that contained nickel sulfate 0.15 M, sodium tungstate 0.10 M, trisodium citrate 0.50 M, boric acid 1.00 M, sodium hydroxide or sulfuric acid to adjust pH to 7.00, as well as with and without 0.05M NaH_2PO_2. The electrodeposition was performed under constant potential and pulse potential deposition modes, and the current was monitored to define the end of the wire or tube growth. The amplitude of the potential in both modes was chosen based on thin film deposit results corresponding to a potential value that should be attributed to the current density of ~ 15 mA cm^{-2} at steady state (the approximation is due to an estimate of membrane porosity.) At this current density, the maximal content of W in the alloys is obtained and the current efficiency is the highest, reducing the gaseous hydrogen evolution. In pulse potential deposition, the value for a relaxation potential (current equal to zero) was set as -0.66 V. The pulse duration was 10 sec, the relaxation duration was 30 sec, and the total number of cycles was 1500. Interesting results showed that while nanowires could be obtained with pulsed deposition, nanotubes were observed in a dc mode, Fig. 12. Nanotubes have also been observed in electrodeposited Co-Ni-Fe-Cu nanotemplated deposits [217, 218] and, similarly, Bi-Te [219]. The tube formation was attributed to the directed potential field along the membrane wall due to mass transport effects, as a consequence of hydrogen evolution. The influence of the side reaction and electrolyte pH was also cited by Fukanaka [220] in the electrodeposition of Ni nanotubes. Nanotubes were observed by Verbeeck [221], too, when depositing Fe nanowires. If short deposition times were used, tubes were formed. They also analyzed the structure and found oxide skins on the nanostructures. The oxygen source was thought to come from the polycarbonate membrane [220, 221].

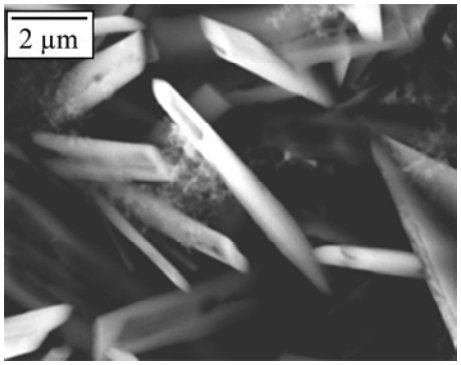

Fig. 12. SEM of Co-W electrodeposits obtained from a citrate-boric acid electrolyte at a constant potential, E =-1.1 V vs SCE [67].

ACKNOWLEDGEMENTS

This work was supported by the FP7 projects NANOALLOY (No. 252407) and TEMADEP (No. 05-104-7540), the MAT2011-27380-C02-01 project from the MINECO (Spain), the US National Science Foundation under Grant No. 0957448, and the Lithuanian ESF agency grant (code VP1-3.1-ŠMM-08-K-01-014).

REFERENCES

1. Lassner E., Schubert W.D. *Tungsten – Properties, Chemistry, Technology of the Element, Alloys, and Chemical Compounds*, Springer, 1999. 422 p.
2. Holt M.L., Kahlenberg L. The Deposition of Tungsten from Aqueous Alkaline Solutions. *Quart. Rev. Am. Electroplaters' Soc*. 1933, **9**, 41–52.
3. Fink G., Jones F.L. The Electrodeposition of Tungsten from Aqueous Solutions. *Trans. Electrochem. Soc.*, 1931, **59**, 461–481.
4. Goltz L.N., Kharlamov V.N. Electrolytic Deposition of Alloys of Tungsten, Nickel and Copper from Water Solutions. *Zhur. Prikl. Khim*., 1936, **9**, 640–652.
5. Schwartz M., Myung N.V., Nobe K. Electrodeposition of Iron Group-rare Earths Alloys from Aqueous Media. *J. Electrochem. Soc*. 2004, **151**, C468–C477.
6. Brenner A., Burkhead P., Seegmiller E. Electrodeposition of Tungsten Alloys Containing Iron, Nickel, and Cobalt. *Journal of Research of the National Bureau of Standards*. 1947, **39**, 351–383.
7. Lietzeke H.M., Holt M.L. Codeposition of Tungsten and Iron from an Aqueous Ammoniacal Citrate Bath. *J. Electrochem. Soc.* 1948, **94**, 252–261.
8. Holt M.L., Vaaler L.E. Electrolytic Reduction of Aqueous Tungstate Solutions, *J. Electrochem. Soc.* 1948, **94,** 50–58.
9. Akiyama T., Fukushima H. Recent Study on the Mechanism of the Electrodeposition of Iron Group Metal Alloys, *ISIJ International*. 1992, **32**, 787–798.

10. Vasko A.T. *Electrochemistry of Tungsten*, Tipogr. Tehnika, Kiev, 1977, 168 p.
11. Brenner A. *Electrodeposition of Alloys. Principle and Practice*. Academic Press, New York and London 1963. 658 p.
12. Bobletsky M., Jordan J. The Metallic Complexes of Tartrates and Citrates, their Structure and Behavior in Dilute Solutions. I. The Cupric and Nickelous Complexes. *J. Am. Chem. Soc.* 1945, **67**, 1824–1831.
13. Bobletsky M., Jordan J. The Structure and Behavior of Ferric Tartrate and Citrate Complexes in Dilute Solutions. *J. Am. Chem. Soc.* 1947, **69**, 2286–2290.
14. Ernst D.W., Amlie R.F., Holt M.L.J. Electrodeposition of Molydenum Alloys from Aqueous Solutions. *J. Electrochem. Soc*. 1955, **102**, 461–469.
15. Ernst D.W., Holt M.L.J. Cathode Potentials During the Electrodeposition of Molybdenum Alloys from Aqueous Solutions. *J. Electrochem. Soc*. 1958, **105**, 686–692.
16. Svensson M., Wahlstrom U., Holmbom G. Compositionally Modulated Cobalt-tungsten Alloys Deposited from a Single Ammoniacal Electrolyte. *Surface and Coatings Technology*. 1998, **105**, 218–223.
17. Wei G.Y., Lou J.W., Ge H.L., Yu Y.D., Jiang L., Sun L.X. Co-W Films Prepared from Electroplating Baths with Different Complexing Agents. *Surface Engineering*. 2012, **28**, 412–417.
18. Weston D.P., Harris S.J., Shipway P.H., Weston N.J., Yap G.N. Establishing Relationships between Bath Chemistry, Electrodeposition and Microstructure of Co-W Alloy Coatings Produced from a Gluconate Bath. *Electrochimica Acta*. 2010, **55**, 5695–5708.
19. Weston D.P., Haris S.J., Capel H., Ahmed N., Shipway P.H., Yellup J.M. Nanostructured Co-W Coa-tings Produced by Electrodeposition to Replace Hard Cr on Aerospace Components. *Transaction of the Institute of Metal Finishing*. 2010, **88**, 47–56.
20. Kapralova I.G., Perelygin Yu.P., Semchenko T.K. Electrodeposition of Nickel-tungsten Alloy from Acetate Electrolyte. *Russian Journal of Applied Chemistry*. 2003, **76**, 1524–1526.
21. Mizushima I., Tang P.T., Hansen H.N., Somers M.A.J. Residual Stress in Ni-W Electrodeposits. *Electrochimica Acta*. 2006, **51**, 6128–6134.
22. Zayats A.I., Perekhrest N.A. Electrodeposition of Iron-tungsten Alloys from Pyrophosphate Electrolytes. *J. Appl. Chem. USSR*. 1971, **44**, 1286–91.
23. Campbell F., Von Fraunhofer J.A. Some Uses of Pyrophosphates in Metal Finishing. Part II. Cobalt-tungsten Alloys to Zinc, Including Pretreatment for Magnesium. *Surface Technology*. 1977, **5**, 235–254.
24. Cesiulis H., Donten M., Donten M.L., Stojek Z. Electrodeposition of Ni-W, Ni-Mo and Ni-Mo-W Alloys from Pyrophosphate Baths. *Materials Science (Medziagotyra)*. 2001, **7**, 237–241.
25. Andricacos P., Boettcher S.H., Malhotra S.G., Paunovic M., Ransom C. Structure Comprising a Barrier Layer of a Tungsten Alloy Comprising Cobalt and/or Nickel. *U.S. Patent Application Publication 6 pp. US 2004108136 A1 20040610 (2004).*
26. Ehrfeld W., Hessel V., Löwe H., Schulz Ch., Weber L. Materials of LIGA Technology. *Microsystem technologies* 1999, **5**, 105–112.
27. Slavcheva E., Mokwa W., Schnakenberg U. Electrodeposition and Properties of NiW Films for MEMS Application. *Electrochimica Acta*. 2005, **50**, 5573–5580.
28. Navarro-Flores E., Chong Z., Omanovic S. Characterization of Ni, NiMo, NiW and NiFe Electroactive Coatings as Electrocatalysts for Hydrogen Evolution in an Acidic Medium. *Journal of Molecular Catalysis A: Chemical*. 2005, **226**, 179–197.
29. Sulitanu N., Brinza F. Structure Properties Relationships in Electrodeposited Ni-W thin Films with Columnar Nanocrystallites. *Journal of Optoelectronics and Advanced Materials.* 2003, **5**, 421–427.
30. Lurje Yu. *Handbook of analytical chemistry*, Khimya, Moscow, 1979, 440 p.
31. Angana Sen, Panchanan Pramanik. A Chemical Synthesis of Fine-grained Metal Tungstate Powders (M=Ca, Co, Ni, Cu, Zn). *Journal of the European Ceramic Society*. 2001, **21**, 745–750.
32. Dias A., Ciminelli V.S.T. Thermodynamic Calculations and Modeling of the Hydrothermal Synthesis of Nickel Tungstates. *Journal of the European Ceramic Society*. 2001, **21**, 2061–2065.
33. Osseo-Asare K. Solution Chemistry of Tungsten Leaching Systems. *Metallurgical and materials transactions B*. 1982, **13**, 555–564.
34. Grith W.P., Lesniak P.J.B. Raman Studies on Species in Aqueous Solutions. Part III. Vanadates, Molybdates, and Tungstates. *J Chem Soc, A.* 1969, **7**, 1066–1071.
35. Pope M.T. Polyoxymetalates. In *Encyclopedia of Inorganic Chemistry*. 2nd Ed. Wiley, 2005, 3966–3976.
36. Aveston J. Hydrolysis of Tungsten (VI): Ultracentrifugation, Acidity Measurements, and Raman Spectra of Polytungstates. *Inorg Chem*. 1964, **3**, 981–986.
37. Contescu C., Jagiello J., Schwartz J.A. Chemistry of Surface Tungsten Species on WO_3/Al_2O_3 Composite Oxides under Aqueous Conditions. *J. Phys Chem*. 1993, **97**, 10152–10157.
38. Kepert D.L. Isopolytungstates. In: *Progress in Inorganic Chemistry (Edited by F.A. Cotton),* 1962, vol. 4, Interscience, New York, 199–274.
39. Kotrly S., Šucha L. *Handbook of Chemical Equilibria in Analytical Chemistry.* Eds Chalmers R.A., Masson M. N.Y.: J. Wiley, 1985. 160 p.
40. Budreika A. The Study of the Electrodeposition of Ni, Co and their Alloys with Tungsten and Molybdenum. *PhD thesis*, Tipogr. Vilnius university, Vilnius, 2010, 116 p.

41. Raghunath C., Lee K.T., Kneer E.A., Mathew V., Raghavan S. Mechanistic Aspects of Chemical Mechanical Polishing of Tungsten Using Ferric Ion Based Glumina Slurries. *Electrochemical Society Proceedings*. 1997, **96–22**, 1–7.
42. Holt M.L., Black R.E. Electrodeposition of Iron-Tungsten Alloys from an Acid Plating Bath. *J. Electrochem. Soc.* 1942, **82**, 205–215.
43. Shacham-Diaman Yosi, Sverdlov D.Y., Petrov N. Electroless Deposition of Thin-Film Cobalt-Tungsten-Phosphorus Layers Using Tungsten Phosphoric Acid ($H_3[P(W_3O_{10})_4]$) for ULSI and MEMS Applications. *J. Electrochem. Soc.* 2001, 148, C162–C167.
44. Cesiulis H., Baltutiene A., Donten M., Donten M.L., Stojek Z. Increase in Rate of Electrodeposition and in Ni(II) Concentration in the Bath as a Way to Control Grain Size of Amorphous/Nanocrystalline Ni-W Alloys. *Journal of Solid State Electrochemistry*. 2002, **6**, 237–244.
45. Cesiulis H., Podlaha-Murphy E.J. Electrolyte Considerations of Electrodeposited Ni-W Alloys for Microdevice Fabrication. *Materials Science (Medziagotyra)*, 2003, 9, 324–327.
46. Donten M., Stojek Z., Cesiulis H. Formation of Nanofibres in thin Layers of Amorphous W Alloys with Ni, Co and Fe Obtained by Electrodeposition. *J. Electrochem. Soc.* 2003, **150**, C95–C98.
47. Donten M., Cesiulis H., Stojek Z. Electrodeposition and Properties of Ni-W, Fe-W and Ni-Fe-W Amorphous Alloys. A Comparative Study. *Electrochimica Acta*. 2000, **45**, 3389–3396.
48. Donten M. Bulk and Surface Composition, Amorphous Structure, and Thermocrystallization of Electrodeposited Alloys of Tungsten with Iron, Nickel, and Cobalt. *J. Solid State Electrochem*. 1999, **3**, 87–96.
49. Easther P., Kennad C.J., Saravanan P., Venkatachalam T. Structural and Magnetic Properties of Electrodeposited Ni-Fe-W thin Films. *Journal of Non-Oxide Glasses*, 2009, **1**, 301–309.
50. Cesiulis H., Budreika A. Electroreduction of Ni(II) and Co(II) from Pyrophosphate Solutions. *Materials Science (Medziagotyra)*. 2010, **16**, 52–56.
51. Cruywagen J.J., Krüger L., Rohwer E.A. Complexation of Tungsten (VI) with Citrate. *Journal of the Chemical Sodiety, Dalton Transactions*. 1991, **7**, 1727–1731.
52. Haseeb A.S.M.A., Albers U., Bade K. Friction and Wear Characteristics of Electrodeposited Nanocrystalline Nickel–tungsten Alloy Films. *Wear*. 2008, **264**, 106–112.
53. Sriraman K.R., Raman S.G.S., Seshadri S.K. Synthesis and Evaluation of Hardness and Sliding Wear Resistance of Electrodeposited Nanocrystalline Ni–W. *Materials Science and Engineering* A. 2006, **418**, 303–311.
54. Yamasaki T. High-strength Nanocrystalline Ni-W Alloys Produced by Electrodeposition. *Materials Physics and Mechanics*. 2000, **1**, 127–132.
55. Zhu L., Younes O., Ashkenasy N., Shacham-Diamand Y., Gileadi E. STM/AFM Studies of the Evolution of Morphology of Electroplated Ni/W alloys. *Applied Surface Science*, 2002, **200**, 1–14.
56. Schuh C.A., Nieh T.G., Iwasaki H. The Effect of Solid Solution W Additions on the Mechanical Properties of Nanocrystalline Ni. *Acta Materialia*. 2003, **51**, 431–443.
57. Donten M., Stojek Z., Osteryoung J.G. Voltammetric, Optical, and Spectroscopic Examination of Anodically Forced Passivation of Co-W Amorphous Alloys. *J. Electrochem Soc*. 1993, **140**, 3417–3424.
58. Donten M., Stojek Z. Pulse Electroplating of Rich-in-tungsten thin Layers of Amorphous Co-W Alloys. *Journal of Applied Electrochemistry*. 1996, **26**, 665–672.
59. Bodaghi A., Hosseini J. Corrosion Behavior of Electrodeposited Cobalt-Tungsten Alloy Coatings in NaCl Aqueous Solution. *Int. J. Electrochem. Sci.* 2012, **7**, 2584–2595.
60. Lietzke M.H., Holt L. Codeposition of Tungsten and Iron from an Aqueous Ammoniacal Citrate Bath. *Journal of the Electrochemical Society*. 1948, **94**, 252–261.
61. Gamburg Yu.D., Zakharov E.N., Goryunov G.E. Electrodeposition, Structure and Properties of Iron-tungsten Alloys. *Russian Journal of electrochemistry.* 2001, **37**, 670–673.
62. Matsunaga M., Li M., Morimitsu M. Mechanism of Electrodeposition of Amorphous Tungsten Alloy Film. *Electrochemical Society Proceedings*, 1998, vol. 97–27, 544–547.
63. Tsyntsaru N., Belevsky S., Dikusar A., Celis J.-P. Tribological Behavior of Electrodeposited Cobalt-Tungsten Coatings: Dependence on Current Parameters. *Trans. Inst. Metal Finish*. 2008, **86**, 301–307.
64. Tsyntsaru N., Cesiulis H., Budreika A., Ye X., Juskenas R., Celis J.-P. The Effect of Electrodeposition Conditions and Post-annealing on Nanostructure of Co–W Coatings. *Surface and Coatings Technology*. 2012, **206**, 4262–4269.
65. Bobanova Zh., Dikusar A.I., Cesiulis H., Celis J.-P., Prosycevas I. Micromechanical and Tribological Properties of Nanocrystalline Coatings of Iron–Tungsten Alloys Electrodeposited from Citrate–Ammonia Solutions. *Russian Journal of Electrochemistry,* 2009, **45**, 895–901.
66. Tsyntsaru N., Dikusar A., Cesiulis H., Celis J.-P., Bobanova Z., Sidel'nikova S., Belevskii S., Yapontseva Y., Bersirova O., Kublanovskii V. Tribological and Corrosive Characteristics of Electrochemical Coatings Based on Cobalt and Iron Superalloys. *Powder Metallurgy and Metal Ceramics*. 2009, **48**, 419–428.
67. Cesiulis H., Xie X.G., Podlaha-Murphy E. Electrodeposition of Co-W Alloys with P and Ni. *Materials Science (Medziagotyra*). 2009, **15**, 115–122.
68. Ibrahim M.A.M., Abd El Rehim S.S., Moussa S.O. Electrodeposition of Noncrystalline Cobalt–tungsten Alloys from Citrate Electrolytes. *Journal of Applied Electrochemistry*. 2003, **33**, 627–633.
69. Eliaz N., Gileadi E. The Mechanism of Induced Codeposition of Ni-W Alloys. *ECS Transactions*. 2007, **2**, 337–349.

70. Younes-Metzler O., Zhu L., Gileadi E. The Anomalous Codeposition of Tungsten in the Presence of Nickel. *Electrochimica Acta*. 2003, **48**, 2551–2562.
71. Younes O., Zhu L., Rosenberg Y., Shacham-Diamand Y., Gileadi E. Electroplating Of Amorphous Thin Films of Tungsten/Nickel Alloys. *Langmuir*. 2001, **17**, 8270–8275.
72. Belevskii S.S., Kosova A.P., Yushchenko S.P., Yakhova E.A., Shul'man A.I., Dikusar A.I. Changes in the Properties of a Citrate Electrolyte Used to Manufacture Cobalt-tungsten Coatings. *Surface Engineering and Applied Electrochemistry*. 2011, **47**, 4–8.
73. Epelboin I., Wiart R. Mechanism of the Electrocrystallization of Nickel and Cobalt in Acidic Solution. *Journal of the Electrochemical Society*, 1971, 118, 1577–1582.
74. Belevskii S.S., Cesiulis H., Tsyntsaru N.I., Dikusar A.I. The Role of Mass Transfer in the Formation of the Composition and Structure of CoW Coatings Electrodeposited from Citrate Solutions. *Surface Engineering and Applied Electrochemistry*. 2010, **46**, 570–578.
75. Bratoeva M., Atanasov N. Effect of Sulfamate-citrate Electrolyte pH on the Ni-W Alloy Electrodeposition. *Russian Journal of Electrochemistry*. 2000, **36**, 60–63.
76. Nishi Y., Mogi Y., Oguri K., Watanabe T. Preparation of Fe-W Amorphous Films by an Electroplating Method. *Journal of Materials Science Letters*. 1995, **14**, 1–3.
77. Ghaferi Z., Raeissi K., Golozar M.A., Edris H. Characterization of Nanocrystalline Co–W Coatings on Cu Substrate, Electrodeposited from a Citrate-ammonia Bath. *Surface and Coatings Technology*. 2011, **206**, 497–505.
78. Younes O., Gileadi E. Electroplating of Ni/WAlloys. I. Ammoniacal Citrate Baths. *J. Electrochem. Soc.* 2002, **149**(2), C100–C111.
79. Clark E., Lietzke M.H. The Mechanism of the Tungsten Alloy Plating Process. *J. Electrochem. Soc.* 1952, **99**, 245–249.
80. Eliaz N., Gileadi E. Induced Codeposition of Alloys of Tungsten, Molybdenum and Rhenium with Transition Metals. *In Modern Aspects of Electrochemistry*, 42 Springer, New York, 2008. 191–301.
81. Aravinda A., Muralidharan V.S., Mayanna S.M. Electrodeposition and Dissolution of Co–W Alloy Films *Journal of Applied Electrochemistry*. 2000, **30**, 601–606.
82. Belevskii S.S., Yushchenko S.P., Dikusar A.I. Anomalous Electrodeposition of Co–W Coatings from a Citrate Electrolyte Due to the Formation of Multinuclear Heterometallic Complexes in the Solution. *Surface Engineering and Applied Electrochemistry.* 2012, **48**, 97–98.
83. Fritz Th., Mokwa W., Schnakenberg U. Electrodeposited Nickel-tungsten Alloys for Micro-engineering. Part I. Deposition Based on Wagramyan Electrolytes. *Galvanotechnik.* 2002, **93**, 2108–2117.
84. Juškėnas R., Valsiūnas I., Pakštas V., Selskis A., Jasulaitienė V., Karpavičienė V., Kapočius V. XRD, XPS and AFM Studies of the Unknown Phase Formed on the Surface During Electrodeposition of Ni–W Alloy. *Applied Surface Science*. 2006, **253**, 1435–1442.
85. Fukusima H., Akiyama T., Akagl S., Higashi K. Role of Iron-group Metals in the Induced Codeposition of Molybdenum from Aqueous Solution. *Transactions of the Japan Institute of Metals*. 1979, **20**, 358–364.
86. Oue S., Nakano H., Kobayashi S., Fukushima H. Structure and Codeposition Behavior of Ni–W Alloys Electrodeposited from Ammoniacal Citrate Solutions. *J. Electrochem. Soc*. 2009, **156**, D17–D22.
87. Chassaing E., Quang K., Wiart R. Mecahnism of Nickel-molybdenum Alloy Electrodeposition in Citrate Electrolytes. *Journal of Applied Electrochemistry*. 1989, **19**, 839–834.
88. Gómez E., Pellicer E., Vallés E. An Approach to the First Stages of Cobalt–nickel–molybdenum, Electrodeposition in Sulphate–citrate Medium. *J. Electroanal. Chem*. 2005, **580**, 222–230.
89. Sun S., Podlaha E.J. Electrodeposition of Mo-rich, MoNi Alloys from an Aqueous Electrolyte. *Journal of the Electrochemical Society*. 2012, **159**, D1–D6.
90. Podlaha E.J., Landolt D. Induced Codeposition: I. Experimental Investigation of Ni-Mo Alloys. *J. Electrochem. Soc.* 1996, **143**, 885–892.
91. Podlaha E.J., Landolt D. Induced Codeposition: II. Mathematical Modeling of Ni-Mo Alloys. *J. Electrochem. Soc.* 1996, **143**, 893–899.
92. Podlaha E.J., Landolt D. Induced Codeposition: III. Molybdenum Alloys with Nickel, Cobalt and Iron. *J. Electrochem. Soc.* 1997, **144**, 1672–1680.
93. Jakŝić J.M., Vojnovic M.V, Krstajic N.V. Kinetic Analysis of Hydrogen Evolution at Ni-Mo Alloy Electrodes. *Electrochimica Acta,* 2000, **45**, 4151–4158.
94. Matlosz M. Competitive Adsorption Effects in the Electrodeposition of Iron-nickel Alloys. *J. Electrochem. Soc.* 1993, **140**, 2272–2279.
95. Baker B.C., West A.C. Electrochemical Impedance Spectroscopy Study of Nickel-iron Deposition: II. Theoretical interpretation. *J. Electrochem. Soc.* 1997, **144**, 169–175.
96. Zech N., Podlaha E.J., Landolt D. Anomalous Codeposition of Iron-Group Alloys. II. Mathematical Model. *J. Electrochem. Soc*. 1999, **146**, 2892–2900.
97. Podlaha E.J., Agarwal P., Landolt D. A Study of the Mo Codeposition Mechanism by Electrochemical Impedance Spectroscopy. *Proceedings of the Symposium on Fundamental Aspects of Electrochemical Deposition and Dissolution Including Modeling*, (Eds. JM. Paunovic, M. Datta, T. Osaka, J. B. Talbot), The Electrochemical Society, Pennington, NJ, 1997, **97–27**, 510–512.

98. Beltowska-Lehman E. Kinetics of Induced Electrodeposition of Alloys Containing Mo from Citrate Solutions. *Physica Status Solidi* (*c*). 2008, **5**, 3514–3517.
99. Obradović M., Stevanović J., Despić A.R., Stevanović R. Electrochemical Deposition and Phase Structure of Electrodeposited Ni-W Alloys. *J. Serb. Chem. Soc.* 1999, **64**, 245–257.
100. Kröger F.A. Cathodic Deposition and Characterization of Metallic or Semiconducting Binary Alloys or Compounds. *J. Electrochem. Soc.*, 1978, 125, 2028–2034.
101. Landolt D. Electrochemical and Materials Science Aspects of Alloy Deposition. *Electrochimica Acta*. 1994, **39**, 1075–1090.
102. Mizushima I., Tang P.T., Hansen H.N., Somers M.A.J. Residual Stress in Ni–W Electrodeposits. *Electrochimica Acta*. 2006, **51**, 6128–6134.
103. Mizushima I., Tang P.T., Hansen H.N., Somers M.A.J. Development of a New Electroplating Process for Ni–W Alloy Deposits. *Electrochimica Acta*. 2006, **51**, 888–896.
104. Donten M., Gromulski T., Stojek Z. The Interface the Interface between Metallic Substrates and Layers of Electrodeposited Co–W Amorphous Alloys. *J. Alloys and Compounds*. 1998, **279**, 272–278.
105. Sulitanu N. Structural Origin of Perpendicular Magnetic Anisotropy in Ni–Wthin Films. *J. Magnetism and Magnet. Mater*. 2001, **231**, 85–93.
106. Vasauskas V., Padgurskas J., Rukuiža R., Cesiulis H., Celis J.-P., Milčius D., Prosyčevas I. Cracking Behavior of Electrodeposited Nanocrystalline Tungsten-cobalt and Tungsten-iron Coatings, *Mechanika.* 2008, **72**, No. 4, 21–27.
107. Ghaferi Z., Raeissi K., Golozar M.A., Saatchi A., Kab S. Comparison of Electrodeposition Aspects and Characteristics of Ni-W and Co-W Alloy Nanocrystalline Coatings. *Iranian Journal of Materials Science & Engineering*. 2010, **7**, 16–24.
108. Yamasaki T., Schlossmacher P., Ehrich K., Ogino Y. Formation of Amorphous Electrodeposited Ni-W Alloys and their Nanocrystallization. *Nanostructured Materials*. 1998, **10**, 375–388.
109. Huang L., Dong J.X., Yang F.Z., Xu S.K., Zhou S.M. Studies on the Mechanism, Structure and Microhardness of Ni–W Alloy Electrodeposits. *Trans. IMF*. 1999, **77**, 185–187.
110. Królikowski A., Płońska E., Ostrowski A., Donten M., Stojek Z. Effects of Compositional and Structural Features on Corrosion Behavior of Nickel–tungsten Alloys. *J. Solid State Electrochem*., 2009, 13, 263–275.
111. Sridhar T.M., Eliaz N., Gileadi E. Electroplating of Ni_4W. *Electrochemical and Solid-State Letters*, 2005, **8**, C58–C61.
112. Yamasaki Y. High-strength Nanocrystalline Ni-W Alloys Produced by Electrodeposition and their Embrittlement Behaviors During Grain Growth. *Scripta mater*. 2001, **44**, 1497–1502.
113. Kimoto Y., Giga A., Ohkubo T., Takigawa Y., Hono K., Higashi K. Ni-W Amorphous/Nanocrystalline Duplex Composite Produced by Electrodeposition. *Materials Transaction*. 2007, **48**, 996–1000.
114. Tsyntsaru N., Bobanova J., Ye X., Cesiulis H., Dikusar A., Prosycevas I., Celis J.-P. Iron–tungsten Alloys Electrodeposited under Direct Current from Citrate–ammonia Plating Baths. *Surface & Coatings Technology.* 2009, **203**, 3136–3141.
115. Younes O., Gileadi E. Electroplating of High Tungsten Content Ni/W Alloys. *Electrochemical Solid-State Letters*. 2000, **3**, 543–545.
116. Zakharov E.N., Gamburg Yu.D., Goryunov G.E., Lyakhov B.F. Effect of Cations of Alkali Metals and Ammonium on the Process of Deposition and Structure of Iron-tungsten Alloys. *Russian Journal of Electrochemistry*. 2006, **42**, 895–900.
117. Pisarek M., Janik-Czachor M., Donten M. Local Characterization of Electrodeposited Ni-W Amorphous Alloy by Auger Microanalysis. *Surface & Coating Technology*. 2008, **202**, 1980–1984.
118. Li H., Li H.X., Deng J-F. The Crystallization Process of Ultrafine Ni-B Amorphous Alloy. *Materials Letters*, 2001, 50, 41–46.
119. Yamasaki T., Schlossmacher P., Ehrlich K., Ogino Y. Nanocrystallization and Mechanical Properties of an Amorphous Electrodeposited $Ni_{75}W_{25}$ Alloy. *Materials Science Forum*, 1998, 269–272, 975–980.
120. Pekala M., Donten M., Stojek Z. Crystallization Study of Amorphous Ni-W Alloys. *Mater. Sci. Eng. A*, 1997, 226–228, 125–127.
121. Capel H., Shipway P.H., Harris S.J. Sliding Wear Behaviour of Electrodeposited Cobalt-tungsten and Cobalt-tungsten-iron Alloys. *Wear* 2003, 255, 917–923.
122. Juskenas R., Valsiunas I., Pakstas V., Giraitis R. On the State of W in Electrodeposited Ni-W Alloys. *Electrochimica Acta*, 2009, 54, 2616–2620.
123. Mun S.-J., Kim M., Yim T.-H., Lee J.-H., Kang T. Mechanical and Structural Characteristics of Electrodeposited Ni–Fe–W Alloy after Heat-treatment. *J.Electrochem. Soc*., 2010, 157, D177–D180.
124. He F.-J., Lei J.-T., Lu X., Huang Y.-N. Friction and Wear Behavior of Electrodeposited Amorphous Fe-Co-W Alloy Deposits. *Trans. Nonferrous Met. Soc. China*, 2004, 14, 901–906.
125. Su F.-H., Huang P. Microstructure and Tribological Property of Nanocrystalline Co-W Alloy Coating Produced by Dual-pulse Electrodeposition. *Materials Chemistry and Physics*. 2012, **134**, 350–359.
126. Hamid A.Z. Electrodeposition of Cobalt–tungsten Alloys from Acidic Bath Containing Cationic Surfactants. *Materials Letters*. 2003, **57**, 2558–2564.
127. Mulukutla M., Kommineni V.K., Harimkar S.P. Pulsed Electrodeposition of Co-W Amorphous and Crystalline Coatings. *Applied Surface Science*. 2012, **258**, 2886–2893.

128. He F., Yang J., Le T., Gu Ch. Structure and Properties of Electrodeposited Fe–Ni–W Alloys with Different Levels of Tungsten Content: A Comparative Study. *Applied Surface Science*. 2007, **253**, 7591–7598.
129. Quiroga A.M.P., Ribotta S.B., Folquer M.E., Gassa L.M., Benitez G., Vela M.E., Salvarezza R.C. Ni–W Coatings Electrodeposited on Carbon Steel: Chemical Composition, Mechanical Properties and Corrosion Resistance. *Electrochimica Acta*. 2011, **56**, 5898–5903.
130. Seong-Jae Mun, Minsoo Kim, Tae-Hong Yim, Jae-Ho Lee, Tak Kanga. Mechanical and Structural Characteristics of Electrodeposited Ni–Fe–W Alloy after Heat-Treatment. *J. Electrochem. Soc*. 2010, **157**, 177–180.
131. Brooman E.W. Wear Behavior of Environmentally Acceptable Alternatives to Chromium Coatings: Cobalt Based and other Coatings. *Metal Finishing.* 2002, **102**, 42–54.
132. Rabinowicz E. *Friction and wear of materials.* Tipogr. John Wiley, New York, 1965, 244 p.
133. Kumar K.S., Van Swygenhoven H., Suresh S. Mechanical Behavior of Nanocrystalline Metals and Alloys. *Acta Materialia*. 2003, **51**, 5743–5774.
134. Buckley D.H. *Surface Effects in Adhesion, Friction, Wear and Lubrication.* In *Tribology series No*. 5, Tipogr. Elsevier, 1981, 631 p.
135. Wang L., Gaoa Y., Xua T., Xuea Q.A Comparative Study on the Tribological Behavior of Nanocrystalline Nickel and Cobalt Coatings Correlated with Grain Size and Phase Structure. *Materials Chemistry and Physics*. 2006, **99**, 96–103.
136. Gamburg Yu.D., Zaharov E.N. The Effect of Hydrogen on Amorfization of Iron-Tungsten Alloys Produced by Electrochemical Synthesis. *Russian J. Electrochem.* 2008, **44**, 736–740.
137. Tsyntsaru N.I., Bobanova Zh.I., Kroitoru D.M., Cheban V.F., Poshtaru G.I., Dikusar A.I. Effect of a Multilayer Structure and Lubrication on the Tribological Properties of Coatings of Fe-W Alloys. *Surface Engineering and Applied Electrochemistry*. 2010, **46**, 538–546.
138. Loewe H., Ehrfeld W., Diebel J. Ultraprecision Microelectroforming of Metals and Metal Alloys. *Proceeding of SPIE, Micromachining and Microfabrication Process Technology III*. 1997, 3223, 168–487.
139. Singh V.B., Singh L.C., Tikoo P.K. Studies on Electrodeposition of Nickel-cobalt-tungsten Alloys. *J. Electrochem. Soc.* 1980, **127,** 590–596.
140. Frantsevich I.N., Teodorovich O.K., Buzhenova L.V., Minakova R.V. Loss of Hardness of the Tungsten-nickel-iron Alloy During Heating. Article II. *Powder Metallurgy and Metal Ceramics*. 1967, **6**, 920–925.
141. Bersirova O., Cesiulis H., Donten M., Krolikowski A., Stoek Z., Baltrunas G. Corrosion and Anodic Behavior of Electrodeposited Ni-Mo Alloys. *Physicochemical Mechanics of Materials*. 2004, (4), 620–625.
142. Safonov V.A., Vykhodtseva L.N., Edigaryan A.A., Aliev A.D., Molodkina E.B., Danilov A.I., Lubnin E.N., Polukarov Y.M. Corrosion-electrochemical Behavior of Chromium Deposits Obtained from Sulfuric Acid Solutions Containing Oxalates. *Russ. J. Electrochem*. 2001, **37**, 127–134.
143. Sinkeviciute J. *Corrosion Study of Electrodeposited W and Mo Alloys with Iron Group Metals*. PhD Theses. Tipogr. Vilnius university, Vilnius, 2009.
144. Elezovic N., Grgur B.N., Krstajic N.V., Jovic V.D. Electrodeposition and Characterization of Fe-Mo Alloys as Cathodes for Hydrogen Evolution in the Process of Chlorate Production. *J. Serb. Chem. Soc.,* 2005, **70**(6), 879–889.
145. Cesiulis H., Budreika A. Hydrogen Evolution and Corrosion of W and Mo Alloys with Co and Ni. *Physicochemical Mechanics of Materials*. 2010, (8), 808–814.
146. Cesiulis H., Sinkevičiūtė J., Bersirova O., Ponthiaux P. Tribocorrosion Testing of Self-passivating Molybdenum and Tungsten Alloys Containing Cobalt and Iron. *BALTTRIB' 2009: Int. Conf. TB, Proceedings*, 2009, 253–258.
147. Hosseini M.G., Abdolmaleki M., Ebrahimzadesh H., Seyed Sadjadi S.A. Effect of 2-butene-1,4-diol on the Nanostructure and Corrosion Resistance Properties of Electrodeposited Ni-W-B Coatings. *Int. J. Electrochem. Sci.* 2011, **6**, 1189–1205.
148. Kublanovsky V., Bersirova O., Dikusar A., Bobanova Zh., Cesiulis H., Sinkeviciute J., Prosycevas I. Electrodeposition and Corrosion Properties of Nanocrystalline Fe-W Alloys. *Physicochemical Mechanics of Materials*. 2008, (7), 308–314.
149. Obradovic M., Stevanovic J., Despic A., Stevanovic R., Stoch J. Characterization and Corrosion Properties of Electrodeposited Ni-W Alloys. *J. Serb. Chem. Soc.* 2001, **66**, 899–912.
150. Galikova Z., Chovancova M., Danielik V. Properties of Ni-W Alloy Coatings on Steel Substrate. *Chem. Pap*. 2006, **60**, 353–359.
151. Tharamani C.N., Beera P., Jayaram V., Begum Noor Shahina, Mayanna S.M. Studies on Electrodeposition of Fe–W Alloys for Fuel Cell Applications. *Applied Surface Science*, 2006, 253, 2031–2037.
152. Yao S., Zhao S., Guo H., Kowaka M. A New Amorphous Alloy Deposit with High Corrosion Resistance. *Corrosion*. 1996, **52**, 183–186.
153. Myung N.V., Park D.-Y., Yoo B.Y., Sumodjo P.T.A. Development of Electroplated Magnetic Materials for MEMS. *Journal of Magnetism and Magnetic Materials*. 2003, **265**, 189–198.
154. Myung N.V., Park D.-Y., Yang H., Schwartz M., Judy J.W., Yang C.-K., Nobe K. Electrodeposited Hard Magnetic thin Films for MEMS Applications. *Proc. Electrochem. Soc.,* 2000, PV2000-29**,** 506–520.
155. Yang H.H., Myung N.V., Lee J., Park D.Y., Yoo B.Y., Schwartz M., Nobe K., Judy J.W. Ferromagnetic Micromechanical Magnetometer. *Sens. Actuators A*. 2002, **97–98**, 88–97.
156. Wei G., Ge H., Zhu X., Wu Q., Yu J., Wang B. Effect of Organic Additives on Characterization of Electrodeposited Co-W thin Films. *Applied Surface Science*, 2007, **253**, 7461–7466.

157. Admon U., Dariel M.P., Gunbaum E., Lodder J.C. Magnetic Properties of Electrodeposited Co-W thin Films. *J. Appl. Phys.* 1987, **62**, 1943–1948.
158. Park D.Y., Ko J.M. Magnetic Properties of Nanocrystalline CoW thin Film Alloys Electrodeposited from Citrate Baths. *J. Korean Electrochem. Soc*. 2003, **6**, 236–241.
159. Sasikumar D., Ganesan S. Effect of Temperature and Current Density in Electrodeposited Co-W Magnetic Nano thin Film. *Dig. J. Nanomater. Bios*. 2010, **5**, 477–482.
160. Chiriac H., Moga A.E., Gherasim C., Lupu N. Preparation and Magnetic Properties of Fe-W and Ni-W Composite Coatings. *Semiconductor Conference*, 2007. CAS 2007. International, 2007, **2,** 307–310.
161. Ge H., Wu Q., Wei G., Wang X., Zhou Q. Effects of Bath Temperature on Electrodeposited Permanent Magnetic Co-Pt-W(P) Films. *Bull. Korean Chem. Soc*. 2007, **28**, 2214–2218.
162. Esther P., Kennady C.J., Saravanan P., Venkatachalam T. Structural and Magnetic Properties of Electrodeposited Ni-Fe-W thin Films. *J. Non-Oxide Glass*. 2009, **1**, 301–309.
163. Franz S., Bestetti M., Consonni M., Cavallotti P.L. Electrodeposition of Micromagnets of CoPtW(P) Alloys. *Microelectron. Eng*. 2002, **64**, 487–494.
164. Ng W.B., Takada A., Okada K. Electrodeposited Co-Ni-Re-W-P thick Array of High Vertical Magnetic Anisotropy. *IEEE Trans. Magn*. 2005, **41**, 3886–3888.
165. Fullerton E.E., Jiang J.S., Bader S.D. Hard/soft Magnetic Heterostructures: Model Exchange-spring Magnets. *J. Magn. Magn. Mater*. 1999, **200**, 392–404.
166. Arul Raj I., Vasu K.I. Transition Metal-based Hydrogen Electrodes in Alkaline Solution –Electrocatalysis on Nickel Based Binary Alloy Coatings. *J. Appl. Electrochem*. 1990, **20**, 32–38.
167. Fan C., Piron D.L., Sleb A., Paradis P. Electrodeposited Nickel-Molybdenum, Nickel-Tungsten, Cobalt-Molybdenum, and Cobalt-Tungsten as Hydrogen Electrodes in Alkaline Water Electrolysis. *J. Electrochem. Soc.* 1994, **141**, 382–387.
168. Kawashima A., Akiyama E., Habazaki H., Hashimoto K. Characterization of Sputter-deposited Ni-Mo and Ni-W Alloy Electrocatalysts for Hydrogen Evolution in Alkaline Solution. *Materials Science and Engineering*: *A*. 1997, **226–228**, 905–909.
169. Marceta Kaninski M.P., Saponjic D.P., Perovic I.M., Maksic A.D., Nikolic V.M. Electrochemical Characterization of the Ni–W Catalyst Formed in Situ During Alkaline Electrolytic Hydrogen Production – Part II. *Applied Catalysis A*. 2011, **405**, 29–35.
170. Wang M., Wang Z., Guo Z., Li Z. The Enhanced Electrocatalytic Activity and Stability of NiW Films Electrodeposited under Super Gravity Field for Hydrogen Evolution Reaction. *Int. J. Hydrog. Energy*. 2011, **36**, 3305–3312.
171. Lua G., Evans P., Zangari G. Electrocatalytic Properties of Ni-Based Alloys Toward Hydrogen Evolution Reaction in Acid Media. *J. Electrochem. Soc*. 2003, **150**, A551–A557.
172. Rashkov R., Arnaudova M., Avdeev G., Zielonka A., Jannakoudakis P., Jannakoudakis A., Theodoridou E. NiW/TiOx Composite Layers as Cathode Material for Hydrogen Evolution Reaction. *Int. J. Hydrog. Energy*. 2009, **34**, 2095–2100.
173. Hu H., Fan Y., Liu H. Hydrogen Production in Single-chamber Tubular Microbial Electrolysis Cells Using Non-precious-metal Catalysts. *Int. J. Hydrog. Energy*, 2009, **34**, 8535–8542.
174. Nenastina T., Bairachnaya T., Ved M., Shtefan V., Sakhnenko N. Electrochemical Synthesis of Catalytic Active Alloys. *Functional Materials*. 2007, **14**, 395–400.
175. Ved M., Shtefan V., Bairachnaya T., Sakhnenko N. New Approach to Catalytic Co-W Alloy Electrodeposition. *Functional Materials*. 2007, **14**, 580–584.
176. Zabinski P.R., Kowalik R., Piwowarczyk M. Cobalt-tungsten Alloys for Hydrogen Evolution in Hot 8M NaOH. *Arch. Metall. Mater*. 2007, **52**, 627–634.
177. Marceta Kaninski M.P., Miulovic S.M., Tasic G.S., Maksic A.D., Nikolic V.M. A Study on the Co–W Activated Ni Electrodes for the Hydrogen Production from Alkaline Water Electrolysis – Energy Sa-ving. *International. Journal of Hydrogen Energy*. 2011, **36**, 5227–5235.
178. Menz W., Bacher W., Harmening M., Michel A. The LIGA Technique – a Novel Concept for Microstructures and the Combination of Si-technologies by Injection Molding. In *IEEE Workshop on Micro Electro Mechanical Systems*, 1991, pp. 69–73. Nara, Japan: IEEE Press.
179. Bley P., Menz W., Bacher W., Feit K., Harmening M., Hein H., Mohr J.,. Schomburg W.K., Stark W. Application of the LIGA Process in Fabrication of Three-dimensional Mechanical Microstructures. In, *MicroProcess 91, 1991 International MicroProcess Conference*, (Eds. S. Namba & T. Tsurushima), 1991, pp. 384–389. Kanazawa, Japan.
180. Romankiw L.T. Electroformation of Electronic Devices. *Plating and Surface Finishing*, 1997, **84**, 10–16.
181. Guckel H., Skrobis K.J., Christenson T.R., Klein J., Han S., Choi B., Lovell E.G. Fabrication of Assembled Micromechanical Components Via Deep X-ray Lithography". In *IEEE Workshop on Micro Electro Mechanical Systems*. 1991, pp. 74–79. Nara, Japan: IEEE Press.
182. Burbaum C., Mohr J., Bley P., Ehrfeld W. Fabrication of Capacitive Acceleration Sensors by the LIGA Technique. *Sensors and Actuators A*. 1991, **25-27**, 559–563.
183. Hemker K.J., Last H. Microsample Tensile Testing of LIGA Nickel for MEMS Applications. *Materials Science and Engineering A*. 2001, **319–321**, 882–886.

184. Buchheit T.E., Lavan D.A., Michael J.R. Leith S.D. Microstructural and Mechanical Properties Investigation of Electrodeposited and Annealed LIGA Nickel Structures. *Metallurgical and Materials Transactions A*. 2002, **33A**, 539–554.
185. Christenson T.R., Buchheit T.E., Schmale D.T., Bourcier R.J. Mechanical and Metallographic Characterization of Liga Fabricated Nickel and 80%Ni-20 %Fe. *Materials Research Society Symposium Proceedings*. 1998, **518**, 185–190.
186. Klement U., Aust K.T., Erb U., El-Sherik M. Thermal Stability of Nanocrystalline Ni. *Material Science and Engineering A*. 1995, **203**, 177–186.
187. Czerwinski F., Szpunar J.A. Controlling the Thermal Stability of Texture in Single-phase Electrodepo-sits. *Nanostructured Materials*. 1999, **11**, 669–676.
188. Cho H.S., Hemker K.J., Lian K., Goettert J. MEMS 2002 Technical Digest. In: *15th IEEE International Conference on MEMS*, 2002, 439–442.
189. Suresha S.J., Haj-Taieb M., Bade K., Aktaa J., Hemker K.J. The Influence of Tungsten on the Thermal Stability and Mechanical Behavior of Electrodeposited Nickel MEMS Structures. *Scripta Materialia*. 2010, **63**, 1141–1144.
190. Haj-Taieb M., Haseeb A.S.M.A., Caulfield J., Bade K., Aktaa J., Hemker K.J. Thermal Stability of Electrodeposited LIGA Ni-W Alloys for High Temperature MEMS Applications. *Microsystem Technologies.* 2008, **14**, 1531–1536.
191. Armstrong D.E.J., Haseeb A.S.M.A., Roberts S.G., Wilkinson A.J., Bade K. Nanoindentation and Micromechanical Fracture Toughness of Electrodeposited Nanocrystalline Ni-W Alloy Films. *Thin Solid Films*. 2012, **520**, 4369–4372.
192. Wang H., Liu R., Cheng F., Cao Y., Ding G., Zhao X. Electrodepositing Amorphous Ni-W Alloys for MEMS. *Microelectronic Engineering*. 2010, **87**, 1901–1906.
193. Podlaha E.J., Namburi L., Murphy M.C. Nickel Alloy Electrodeposited Microstructures. *Patent Application Publication No. US-2004-0011432-A1*, 2004.
194. Ross C.A. Electrodeposited Multilayer thin Films. *Annual Review of Material Science*. 1994, 24, 159–188.
195. Schwarzacher W., Lashmore D.S. Giant Magnetoresistance in Electrodeposited Films. *IEEE Transactions on Magnetics*. 1996, **32**, 3133–3153.
196. Alper M. Electrodepozition of Multilayered Nanostructures. *Nanostructured Magnetic Materials and their Applications*. Lecture Notes in Physics, V. 593. D. Shi, B. Aktas, L. Pust, F. Mikailov (Eds.), pp.11–128, Springer, Berlin (2002).
197. Fert A., Barthelemy A., Galtier P., Holody P., Loloee R., Morel R., Petroff F., Schroeder P., Steren L.B., Valet T. Giant Magnetoresistance in Magnetic Nanostructures. Recent developments. *Material Science and Engineering*: *B*. 1995, **31**, 1–9.
198. Lee S.F., Pratt W.P., Yang Q., Holody P., Loloee R., Schroeder P.A. Bass J. Two-Channel Analysis of CPP-MR Data for Ag/Co and AgSn/Co Multilayers. *Journal of Magnetism and Magnetic Materials*. 1993, **118**, L1–L5.
199. Pratt W.P., Lee S.F., Holody P., Yang Q., Loloee R., Bass J., Schroeder P.A. Giant Magnetoresistance with Current Perpendicular to the Multilayer Planes. *Journal of Magnetism and Magnetic Materials*. 1993, **126**, 406–409.
200. Liu K., Nagodawithana K., Searson P.C., Chien C.L. Perpendicular Giant Magnetoresistance of Multilayered Co/Cu Nanowires. *Physical Review B*. 1995, **51**, 7381–7385.
201. Blondel A., Doudin B., Ansermet J.-P. Comparative Study of the Magnetoresistance of Electrodepo-sited Co/Cu Multilayered Nanowires Made by Single and Dual Bath Techniques. *Journal of Magnetism and Magnetic Materials*. 1997, **165**, 34–37.
202. Piraux L., George J.M., Despres J.F., Leroy C., Ferain E., Legras R., Ounadjela K., Fert A. Giant Magnetoresistance in Magnetic Multilayered Nanowires. *Applied Physics Letters*. 1994, **65**, 2484–2487.
203. Dubois S., Beuken J.M., Piraux L., Duvail J.L., Fert A., George J.M., Mauric J.L. Perpendicular Giant Magnetoresistance of NiFe/Cu and Co/Cu Multilayered Nanowires. *Journal of Magnetism and Magnetic Materials*. 1997, **165**, 30–33.
204. Piraux L., Dubois J.S., Duvail J.L., Ounadjela K., Fert A. Arrays of Nanowires of Magnetic Metals and Multilayers: Perpendicular GMR and Magnetic Properties. *Journal of Magnetism and Magnetic Materials*. 1997, **175**, 127–136.
205. Pullini D., Busquets D., Ruotolo A., Innocenti G., Amigo V. Insights into Pulsed Electrodeposition of GMR Multilayered Nanowires. *Journal of Magnetism and Magnetic Materials*. 2007, (16), e242–e245.
206. Evans P.R., Yi G., Schwarzacher W. Current Perpendicular to Plane Giant Magnetoresistance of Multilayered Nanowires Electrodeposited in Anodic Aluminum Oxide Membranes. *Applied Physics Letters*. 2000, **76**, 481–484.
207. Schwarzacher W., Attenborough K., Michel A., Nabiyouni G., Meier J.P. Electrodeposited Nanostructures. *Journal of Magnetism and Magnetic Materials*. 1997, **165**, 23–29.
208. Schwarzacher W., Kasyutich O.I., Evans P.R., Darbyshire M.G., Yi G., Fedosyuk V.M., Rousseaux F., Cambril E., Decanini D. Metal Nanostructures Prepared by Template Electrodeposition. *Journal of Magnetism and Magnetic Materials*. 1999, **198–199**, 185–190.
209. Wang Y.W., Wang G.Z., Wang S.X., Gao T., Sang H., Zhang L.D., Fabrication and Magnetic Properties of Highly Ordered Co16Ag84 Alloy Nanowire Array. *Applied Physics A: Materials Science & Processing*. 2002, **74**, 577–580.
210. Wang Y.W., Zhang L.D., Meng G.W., Peng X.S., Jin X.Y., Zhang J. Fabrication of Ordered Ferromagnetic-Nonmagnetic Alloy Nanowire Arrays and their Magnetic Property Dependence on Annealing Temperature. *Journal of Physical Chemistry B*. 2002, **106**, 2502–2507.
211. Liu Q.F., Gao C.X., Xiao J.J., Xue D.S. Size Effects on Magnetic Properties in $Fe_{0.68}$ $Ni_{0.32}$ Alloy Nanowire Arrays. *Journal of Magnetism and Magnetic Materials*. 2003, **260**, 151–155.

212. Qin D.H., Wang C.W., Sun Q.Y., Li H.L. The Effects of Annealing on the Structure and Magnetic Properties of CoNi Patterned Nanowire Arrays. *Applied Physics A: Materials Science & Processing*. 2002, **74**, 761–765.
213. Kazeminezhad I., Schwarzacher W. Electrodeposition of NiCu Alloy Nanowires with Arbitrary Composition. *Electrochemical and Solid State Letters*. 2004, **11**, K24–K26.
214. Huang Q., Davis D., Podlaha E.J. Electrodeposition of FeCoNiCu Nanowires. *Journal of Applied Electrochemistry*. 2006, **36**, 871–882.
215. Gupta M., Podlaha E.J. Electrodeposition of CuNiW Alloys: thin Films, Nanostructured Multilayers and Nanowires. *Journal of Applied Electrochemistry*, 2010, **40**, 1429–1439.
216. Bairachna T., Fowle W., Podlaha E.J. Electrochemically Fabricated Nickel-Tungsten Nanowires. *ECS Transactions, 220th Meeting of The Electrochemical Society, Boston, MA, Oct, 2011.*
217. Davis D., Zamanpour M., Moldovan M., Young D., Podlaha E.J. Electrodeposited, GMR CoNiFeCu Nanowires and Nanotubes from Electrolytes Maintained at Different Temperatures. *Journal of the Electrochemical Society*. 2010, **157**, D317–D322.
218. Davis D., Moldovan M., Young D., Xie X., Henk M., Podlaha E.J. Magnetoresistance in Electrodeposited CoNiFe/Cu Multilayered Nanotubes Electrochemical/Chemical Deposition and Etching. *Electrochemical and Solid State Letters*. 2006, **9**, C153–C155.
219. Pinisetty D., Davis D., Podlaha-Murphy E.J., Murphy M.C., Karki A.B., Young D.P., Devireddy R.V. Characterization of Electrodeposited Bismuth-Tellurium Nanowires and Nanotubes. *Acta Materialia*. 2011, **59**, 2455–2461.
220. Fukunaka Y., Motoyama M., Konishi Y., Ishii R. Producing Shape-Controlled Metal Nanowires and Nanotubes by an Electrochemical Method Electrochemical/Chemical Deposition and Etching. *Electrochemical and Solid-State Letters*. 2006, **9**, C62–C64.
221. Verbeeck J., Lebedev O.I., Van Tendeloo G., Cagnon L., Bougerol C. Fe and Co Nanowires and Nanotubes Synthesized by Template Electrodeposition: A HRTEM and EELS Study. *Journal of the Electrochemical Society*. 2003, **150**, E468–E471.

Received 17.01.12

Реферат

Теоретические и прикладные исследования сплавов вольфрама с металлами группы железа (Me-W) проводятся во всем мире ввиду их разностороннего применения. Целью данной статьи является обзор исследований по электроосаждению сплавов вольфрама с металлами группы железа, их свойств и применения. На основе 221 работы, обзор сфокусирован на следующих теоретических и практических направлениях: химии электролитов для электроосаждения, механизмов соосаждения и свойств электроосажденных сплавов вольфрама. Также, приводится анализ образования комплексов W (VI) и с металлами (Me) группы железа (поливольфраматов и комплексов Me (II) и W (VI)) с цитратами и гидроксогруппами на основе опубликованных данных и рассчитано распределение разных комплексов металла группы железа и вольфрама в зависимости от pH (от 1 до 10) для электролитов в присутствии/отсутствии цитратов. Приведена корреляция между комплексным составом электролитов и составом электроосажденных сплавов. Кроме того, критически рассматриваются описанные в литературе различные модели соосаждения вольфрама с металлами группы железа. Также рассмотрены особенности строения сплавов вольфрама и их термостойкость, механические, трибологические и магнитные свойства, коррозия сплавов, их применение в электрокатализе выделения водорода, темплатного осаждения с целью получения микро- и наноструктур.